Journal of Medicinal Chemistry



Article

# Discovery of selective inhibitors targeting acetylcholinesterase 1 from disease-transmitting mosquitoes

Cecilia Engdahl, Sofie Knutsson, Fredrik J. Ekström, and Anna Linusson

*J. Med. Chem.*, **Just Accepted Manuscript** • DOI: 10.1021/acs.jmedchem.6b00967 • Publication Date (Web): 06 Sep 2016



## Just Accepted



ACS Publications

Journal of Medicinal Chemistry is published by the American Chemical Society. 1155 Sixteenth Street N.W., Washington, DC 20036

# Discovery of selective inhibitors targeting acetylcholinesterase 1 from disease-transmitting mosquitoes

*Cecilia Engdahl,[†,$] Sofie Knutsson,[†,$] Fredrik Ekström,[‡*] and Anna Linusson[†*]*

†Department of Chemistry, Umeå University, SE-90187 Umeå, Sweden

‡Swedish Defense Research Agency, CBRN Defense and Security, SE-906 21 Umeå, Sweden

* Corresponding author

$ These authors contributed equally

E-mail address: anna.linusson@umu.se; fredrik.ekstrom@foi.se

ABSTRACT

Vector control of disease-transmitting mosquitoes is increasingly important due to the re-emergence and spread of infections such as malaria and dengue. We have conducted a high throughput screen (HTS) of 17,500 compounds for inhibition of the essential AChE1 enzymes from the mosquitoes *Anopheles gambiae* and *Aedes aegypti*. In a differential HTS analysis

including the human AChE, several structurally diverse, potent, and selective non-covalent AChE1 inhibitors were discovered. For example, a phenoxyacetamide-based inhibitor was identified with a 100-fold selectivity for the mosquito- over the human enzyme. The compound also inhibited a resistance conferring mutant of AChE1. Structure-selectivity relationships could be proposed based on the enzymes' 3D structures; the hits' selectivity profiles appear to be linked to differences in two loops that affect the structure of the entire active site. Non-covalent inhibitors of AChE1, such as the ones presented here, provide valuable starting points towards insecticides and are complementarity to existing and new covalent inhibitors.

## INTRODUCTION

Mosquitoes act as vectors for parasitic and viral infectious diseases such as malaria, dengue, chikungunya, Zika infection, and lymphatic filariasis that affect the health of hundreds of millions of people every year. Many previously controlled vector-borne diseases are re-emerging or spreading to new parts of the world, partly because of globalization and climate change.[1-2] For example, dengue is one of the fastest spreading vector-borne diseases and is now considered a serious public health threat with 40% of the world's population at risk.[2-4] The incidence of the deadliest vector-borne disease, malaria, has declined following a massive global effort over the last fifteen years, but 1.2 billion people remain at high risk of infection.[5-6] International initiatives and campaigns aiming to increase the coverage of current mosquito-control interventions, which are primarily based on insecticide-treated bed nets (ITN) and indoor residual spraying (IRS), have helped to significantly reduce the risk of malaria in Sub-Saharan Africa.[5-6] These methods currently rely on four chemical classes of insecticides that are recommended by the World Health Organization (WHO) for mosquito vector control purposes: chlorinated hydrocarbons,

organophosphates, carbamates, and pyrethroids (Figure 1). All of them are recommended for IRS while only the pyrethroids are recommended for treatment of bed nets. The insecticidal effects on the targeted organisms are similar for all chemicals; interference with the nervous system which causes paralysis and death of the mosquitoes.[7]

While the large-scale production and widespread use of insecticides has had beneficial effects in terms of disease control and crop protection it has also caused the insecticides to accumulate in ecosystems, with harmful effects on non-target species including humans.[7-9] Moreover, it has promoted the development and spread of insecticide-resistant mosquito populations.[10-13] Consequently, there is a need for new vector control strategies, ideally based on combinations of different approaches, such as biopesticides (i.e. microorganisms, viruses, or natural products that target insect vectors) and insecticides with novel mode of actions.[14-17]

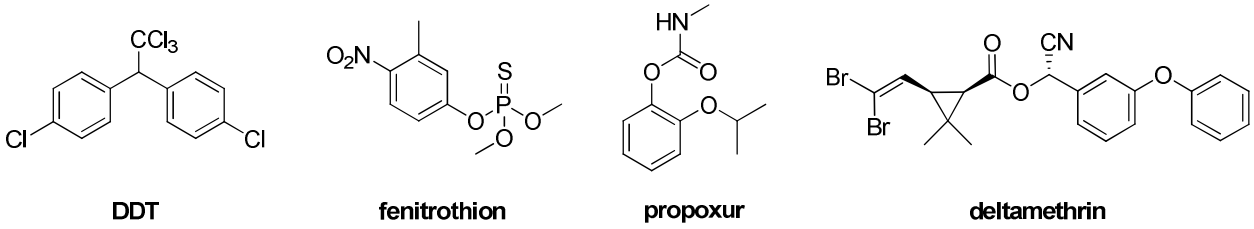


DDT fenitrothion propoxur deltamethrin

**Figure 1.** Some representative insecticides currently used for vector control. From the left: the chlorinated hydrocarbon DDT, the organophosphate fenitrothion, the carbamate propoxur, and the pyrethroid deltamethrin.

The organophosphate and carbamate insecticides target the essential enzyme acetylcholinesterase (AChE, EC 3.1.1.7) through a covalent modification of the catalytic serine residue.[8, 18-19] AChE terminates cholinergic transmission through a rapid hydrolysis of the neurotransmitter acetylcholine. Inhibition of AChE causes an accumulation of acetylcholine,

leading to an overstimulation of the nervous system. While current insecticides are very efficient at controlling disease-transmitting mosquitoes, the compounds are non-specific and inhibit AChE enzymes from many different species including humans.[19-20] In addition, insecticide insensitive mosquito strains have evolved in several species. Various mutations of mosquito-AChE1 that confer resistance to existing insecticides have been reported in literature. The most abundant and well-studied mutations are the G122S substitution (human AChE (*h*AChE) numberings are used throughout the text; G122S corresponds to G119S in *Torpedo californica* AChE (*Tc*AChE)) found in *Anopheles gambiae* and *Culex pipiens* among others,[21] the F338W (F331W in *Tc*AChE) in *Culex triaeniorhynchus*,[22] and the F297V (F290V in *Tc*AChE) in *Culex pipiens*.[23]

Mosquitoes have two genes encoding AChE enzymes: *ace-1* and *ace-2,* expressing the AChE1 and AChE2 enzymes, respectively,[24-26] while vertebrates have only one gene. In mosquitoes, AChE1 is the isoform responsible for AChE-mediated insecticide resistance and also have higher catalytic activity than AChE2.[21, 27] The role of AChE2 is still not fully understood. In this work we are focusing on AChE1 from *Anopheles gambiae* (*Ag*AChE1; vector of the malaria parasite) and *Aedes aegypti* (*Aa*AChE1; vector of the dengue, yellow fever, Zika, and chikungunya viruses). Both the AChE1 and AChE2 enzymes from *Anopheles gambiae* and *Aedes aegypti* share many functional and structural characteristics with vertebrate AChEs.[28-33] For example, sequence comparisons, crystallographic studies of enzymes from various species, and homology modelling of *Ag*AChE1 suggest that the overall three dimensional structures of vertebrate and mosquito enzymes are similar.[30, 34-36]

Despite the similarities between vertebrate and mosquito AChEs, promising covalent inhibitors of mosquito AChE1 have been obtained using two different design strategies; modification of an free cysteine unique for insect AChEs[36-40] and modification of the catalytic serine residue using reversible covalent inhibitors.[20, 30, 41-46] Both strategies have yielded covalent inhibitors displaying

selectivity for mosquito AChE1 over *h*AChE[38, 40-41] and other non-target organisms.[20, 46] In a recent functional comparison of AChEs from vertebrates (*h*AChE and *Mus musculus* AChE (*m*AChE)) and mosquitoes (*Ag*AChE1 and *Aa*AChE1) we have showed small but significant differences in ligand binding properties for non-covalent inhibitors as well.[33] Also the resistance conferring G122S mutant of *Ag*AChE1 (G122S-*Ag*AChE1) has been targeted by both carbamate-based covalent inhibitors[42-45] and non-covalent inhibitors.[47]

To explore non-covalent inhibitors of mosquito AChE1 on a larger scale, we here present a high throughput screening (HTS) of a library comprising 17,500 compounds. The hits' chemical diversity and potential selectivity were investigated in a differential HTS study in which the screening results for the mosquito AChE1s were compared with previously reported data from the human enzyme.[48] We also present the synthesis and biochemical evaluation, including G122S-*Ag*AChE1, of two hits with different selectivity profiles and present structure-selectivity analyses for both compounds based on three dimensional protein-ligand complex structures.

## RESULTS

### Discovery of *Ag*AChE1 and *Aa*AChE1 inhibitors

To identify inhibitors of *Ag*AChE1 and *Aa*AChE1, we adapted the activity-based colorimetric Ellman assay[49] to a format suitable for screening of 17,500 compounds at a single concentration. The performance of the screening campaign was monitored by repeated runs of a reference plate containing eight compounds with different inhibition capacities, for example the previously characterized compound **1** (Table 1).[33, 48] The developed assay proved to be robust; it exhibited a good ability to distinguish between active and inactive compounds, having satisfying average Z'-factors[50] of 0.65 and 0.73 for *Ag*AChE1 and *Aa*AChE1, respectively (see Supporting Information, Figures S1-S7, Tables 1-3). On the basis of the reference plate analyses, the proportions of false

positives for the HTS campaigns were estimated to be 6% and 11% for *Ag*AChE1 and *Aa*AChE1, respectively; the proportion of false negatives was estimated to be 0.5% for both enzymes.

The AChE1 screens identified 338 compounds that significantly reduced the activity of *Ag*AChE1, *Aa*AChE1, or both proteins (henceforth, AChE1 is used to refer to either or both of *Ag*AChE1 and *Aa*AChE1) at a concentration of 50 μM. The identified hits inhibited the enzymes' ability to hydrolyse the substrate by 33-98% in the case of *Ag*AChE1 and 31-96% for *Aa*AChE1 at the tested concentration; the overall hit rates for the two enzymes were 1.3% and 1.6%, respectively. The inhibition profiles of *Ag*AChE1 and *Aa*AChE1 derived from our screening studies indicated that the two mosquito enzymes behaved very similar: only 35 of the 338 screening hits exhibited appreciable differences in their capacity to inhibit *Ag*AChE1 and *Aa*AChE1.

We next confirmed the hits' inhibitory activity by determining their half maximal inhibitory concentrations ($IC_{50}$) for *Ag*AChE1 and *Aa*AChE1 (Table 2). $IC_{50}$ values based on freshly prepared stock solutions were determined for 61 of the screened compounds that had different physicochemical properties and represented three different activity ranges of AChE1 (set A: 70-100% inhibition; set B: 31-69% inhibition; set C: ≤ 30% inhibition; see Supporting Information, Tables S4 and S5 and Figures S8-S17). In addition, a fourth set of 15 hits was re-tested. This last set was selected from the group of compounds showing different inhibitory activity towards *Ag*AChE1 and *Aa*AChE1 (set $D_1$-$D_2$: ≥ 30% difference in measured inhibition). The chemical structures of nine of the studied compounds and the corresponding inhibition data are presented in Table 1 (the complete inhibition results for all the re-tested compounds can be found in the Supporting Information, Table S6). The results of this full dose-response analysis generally agreed well with the screening data. A good correlation between the inhibition at a single

concentration and the corresponding $IC_{50}$ value was also reported in the previous HTS targeting *h*AChE.[48]

**Table 1.** Reference compound **1** and selected compounds from sets A-D with their HTS inhibition and dose-response data.

| C | Set | Structure | HTS (% inhibition) | | $IC_{50}$ (μM)[a] | | | |
|---|---|---|---|---|---|---|---|---|
| | | | *Ag* | *Aa* | *Ag* | *Aa* | *h* | S.R[b] |
| **1** | R | 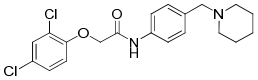 | 93 | 91 | 0.26 (0.13-0.52) | 0.44 (0.17-1.1) | 0.030 (0.028-0.034) | 0.07 |
| **2** | A | 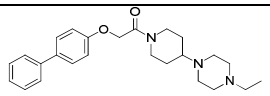 | 92 | 76 | 0.21 (0.12-0.37) | 0.22 (0.12-0.38) | 31 (29-34) | 141 |
| **3** | A | 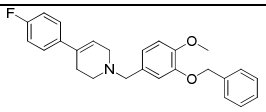 | 86 | 90 | >100 | >100 | >200 | n.a. |
| **4** | A | 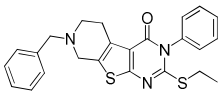 | 94 | 93 | 8.3 (6.8-10) | 8.8 (7.1-11) | 5.1 (4.4-6.0) | 0.6 |
| **5** | A | 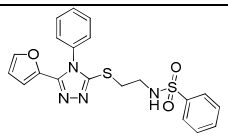 | 76 | 82 | >1000 | >1000 | >1000 | n.a. |
| **6** | B | 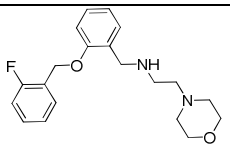 | 23 | 38 | >500 | >500 | >500 | n.a. |
| **7** | B | 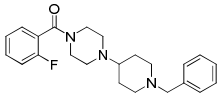 | 32 | 33 | 17 (12-22) | 12 (9.6-14) | >200 | >12 |

| | | | | | | | | |
|---|---|---|---|---|---|---|---|---|
| **8** | C | 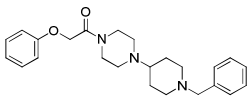 | 24 | 18 | 21 (19-23) | 19 (17-20) | 43 (41-46) | 2 |
| **9** | D1 | 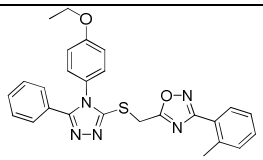 | 63 | 1 | >1000 | >1000 | >1000 | n.a. |
| **10** | D2 | 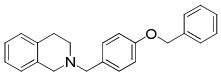 | 41 | 80 | 2.9 (1.6-5.2) | 2.9 (2.0-4.2) | >200 | >67 |

[a]$IC_{50}$ values were determined using 2 replicates. The 95% confidence interval is given in parentheses. [b]Selectivity ratios were computed by taking the compound's $IC_{50}$ value against *h*AChE and dividing by the higher of its $IC_{50}$ values against *Ag*AChE1 and *Aa*AChE1. n.a. refers to not applicable.

Of the 76 compounds tested in the follow up assays, more than half inhibited AChE1 with $IC_{50}$ values ranging from 0.2 to 128 μM (Table 2). The remainder had $IC_{50}$ values above 200 μM, or showed a poor solubility, preventing a full dose-response analysis. All but three of the compounds in set A inhibited AChE1 in a dose-dependent manner. This group included the inhibitors that showed the highest potency, such as compound **2** which had $IC_{50}$ values of 0.21 μM and 0.22 μM for inhibition of *Ag*AChE1 and *Aa*AChE1, respectively (Table 1, Supporting Information, Table S6). Several of the hits in set B were also confirmed to be inhibitors, with $IC_{50}$ values between 2.4 and 22 μM. However, the false positive rate for this group appeared to be higher than that for set A. Four of the compounds from set C proved to be false negatives and showed dose-dependent inhibition of AChE1. These four inhibitors had similar structures to some compounds from sets A and B but were generally less potent than their analogues, having $IC_{50}$ values ranging from 11-128 μM (compared to 0.21-22 μM for compounds from the first two sets). The $IC_{50}$ data for the compounds in set D showed that none of them were significantly more active against one mosquito enzyme than the other. In fact, most of these compounds were false

positives: only two were active inhibitors, and both of them were equally potent against *Ag*AChE1 and *Aa*AChE1.

**Table 2.** HTS and dose-response data for selected compounds from the screening campaigns targeting *Ag*AChE1 and *Aa*AChE1.

| | **Set A**[a,b] | **Set B**[a,c] | **Set C**[a,d] | **Set D1**[a,e] | **Set D2**[a,f] |
|---|---|---|---|---|---|
| **No. of tested compounds** | 24 | 23 | 14 | 9 | 6 |
| **HTS inhibition *Ag*AChE1 (%)** | 61 - 96 | 13 - 66 | -21 - 24 | 37 - 63 | -40 - 41 |
| **HTS inhibition *Aa*AChE1 (%)** | 72 - 96 | 25 - 69 | -11 - 25 | -5 - 2 | 47- 80 |
| **Confirmed inhibitors of AChE1** | 21 | 13 | 4 | 0 | 2 |
| **$IC_{50}$ *Ag*AChE1 (µM)** | 0.21 - 86 | 2 - 22 | 11 - 73 | - | 3 - 7 |
| **$IC_{50}$ *Aa*AChE1 (µM)** | 0.22 - 66 | 2 - 19 | 12 - 128 | - | 2 - 6 |
| **$IC_{50}$ AChE1 (> 200µM)** | 3 | 6 | 8 | 9 | 2 |
| **nd**[g] | 0 | 4 | 2 | 0 | 2 |

[a]If a hit fell into one activity group for one enzyme and a different activity group for the other, it was assigned to the group corresponding to its highest level of inhibition. [b]Hits showing ≥70% inhibition in the HTS. [c]Hits showing 31-69% inhibition in the HTS. [d]Hits showing ≤ 30% inhibition in the HTS. [e]Hits showing ≥ 30% higher inhibition of *Ag*AChE1 than *Aa*AChE1. [f]Hits showing ≥ 30% higher inhibition of *Aa*AChE1 than *Ag*AChE1. [g]Could not be determined due to poor solubility.

**Chemical diversity and selectivity of AChE1 inhibitors**

The discovery of potent AChE1 inhibitors prompted us to further analyse the data from the two screens against AChE1 and the previously reported HTS targeting *h*AChE[48] (i.e. differential HTS analysis). The assay conditions for the three screens were comparable (e.g. plate format, buffer conditions, substrate- and compound concentrations) and each screening was evaluated based on

its own statistics. Combining the HTS hits for AChE1 and *h*AChE yielded 425 unique hits. An investigation of the AChE1- and *h*AChE hits revealed that both sets consisted of chemically diverse compounds that were similar with respect to their overall molecular size, hydrophobicity, and flexibility: the MW values for the AChE1 and *h*AChE hits ranged from 199-629 and 234-596, respectively; their logP values were between 0.6-8.7 and -1.2-8.1, respectively; and their numbers of rotatable bonds were between 0-10 and 0-12, respectively. Many of the compounds contained a basic amine capable of forming activated CH···arene interactions, which are commonly observed in AChE-inhibitor complexes.[51] However, the sets of AChE1 and *h*AChE hits also included some neutral and anionic inhibitors.

Interestingly, comparisons of the HTS data showed that only 10% of the AChE1 hits were also scored as hits against *h*AChE. Mosquito over human selectivity was further investigated by determining the $IC_{50}$ values of the compounds from sets A-D for inhibition of *h*AChE (Table 1, Supporting information, Table S6). Indeed, the full dose-response analysis agreed with the data from the HTS and many of the compounds were confirmed to be selective for AChE1 over *h*AChE; 26 compounds were identified with $IC_{50}$ values for AChE1 that were at least a factor ten lower than the corresponding value for *h*AChE. This finding shows that the mosquito and human enzymes have different preferences for different chemotypes. In addition, this analysis also demonstrated that it was possible to identify potentially AChE1 selective hits on the basis of their inhibition (%) in the HTS (Table 1, Supporting Information, Table S6). Hits with more than a fivefold higher inhibition potency in the HTS also had $IC_{50}$-based selectivity ratios ($S.R._{IC50}$ values) of ten or more.

Analysis of the HTS data from the three screens showed that the combined set of AChE1- and *h*AChE hits contained 163 AChE1 selective hits, 74 *h*AChE selective hits and 37 non-selective

hits (see Experimental Section for selectivity criteria). The remaining hits were classified as miscellaneous. A multivariate regression discriminant analysis of the selective AChE1- and *h*AChE hits based on selected molecular descriptors indicated chemical differences between the two groups of compounds. The analysis showed that the AChE1 selective hits were smaller, more flexible, and had a larger fraction of saturated hydrocarbons than the *h*AChE selective hits (see Supporting Information, Tables S7 -S8 and Figure S19).

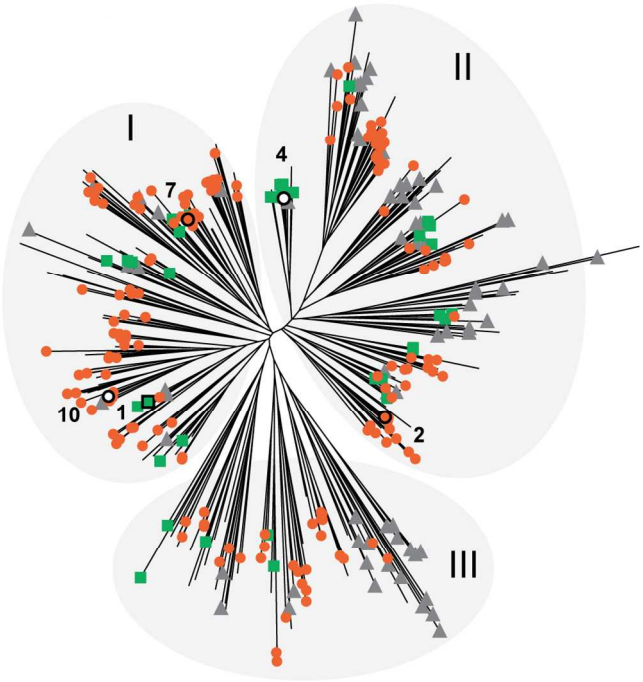


**Figure 2.** Chemical structural tree of the 425 AChE1 and *h*AChE hits. Three major classes (I-III) of hits are shown, each against a grey background. Based on the HTS-data, hits showing potential selectivity for AChE1 are shown as orange dots, non-selective hits as green squares, and hits showing potential selectivity for *h*AChE as grey triangles, while non-marked hits were miscellaneous. Compounds **1**, **2, 4**, **7**, and **10** are labeled and their symbols are outlined in black.

The hits' chemical diversity and selectivity were investigated further by performing a cluster analysis of their structural fingerprints and selectivity profiles, yielding the chemical structural tree shown in Figure 2. The tree revealed three major groups of hit structures (I-III); the first contained more flexible compounds, the second had high contents of heteroatoms (N, O, and S), and the last contained hits with higher contents of aromatic and/or rigid substructures. Mapping the compounds' selectivity profiles onto the tree revealed clusters of similar molecules that had distinct effects on the studied enzymes – one type comprising compounds with high potential selectivity for AChE1, another comprising compounds with high potential selectivity for *h*AChE, and a third comprising compounds with mixed selectivity profiles (Figure 2). For example, compounds **2**, **7**, and **10** belonged to clusters in which most of the compounds showed potential selectivity for AChE1 while compounds **1** and **4** belonged to clusters in which the hits were potentially non-selective or exhibited mixed selectivity. Compounds **2** and **7** had high selectivity ratios ($S.R._{IC50} > 12$) indicating preferential inhibition of AChE1, while compound **1**, which shares a number of structural features with **2** and **7**, was potent against all three enzymes. To better understand the selectivity properties of AChE1 and *h*AChE, we decided to further investigate the highly potent and AChE1 selective compound **2**, and the chemically similar but non-selective **1**.

**Synthesis and biochemical evaluation of 2 and 1**

Compound **2** was prepared in two steps as outlined in Scheme 1 by performing a Williamson ether synthesis with 4-phenylphenol (**11)** and chloroacetic acid to give **12** followed by an amide coupling with 1-ethyl-4-pipiridin-4-yl piperazine, using TBTU as the coupling reagent. The synthesis of **1** was accomplished by nucleophilic substitution of 4-nitrobenzyl bromide (**13)** with piperidine followed by reduction to yield the corresponding aniline **15**. Coupling of this

intermediate with chloroacetic acid chloride provided the desired amide **16,** allowing the final compound **1** to be obtained by ether formation with 2,4-dichlorophenol (Scheme 2).

**Scheme 1**[a]

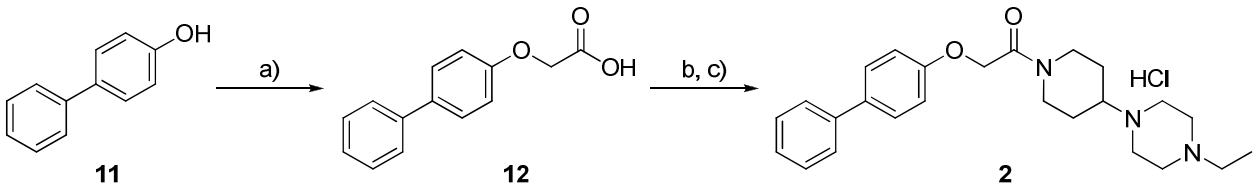


[a]Reagents and conditions: (a) chloroacetic acid (5 eq), NaOH (s) (7 eq), MeOH, reflux 24h, yield 29% (b) 1-ethyl-4-piperidin-4-yl-piperazine (1.2 eq), TBTU (1.2 eq), TEA (3 eq), DMF, rt 5 days (c) Half sat. HCl in $CH_2Cl_2$, 0 °C to rt, 20h, yield 47% over two steps.

**Scheme 2**[a]

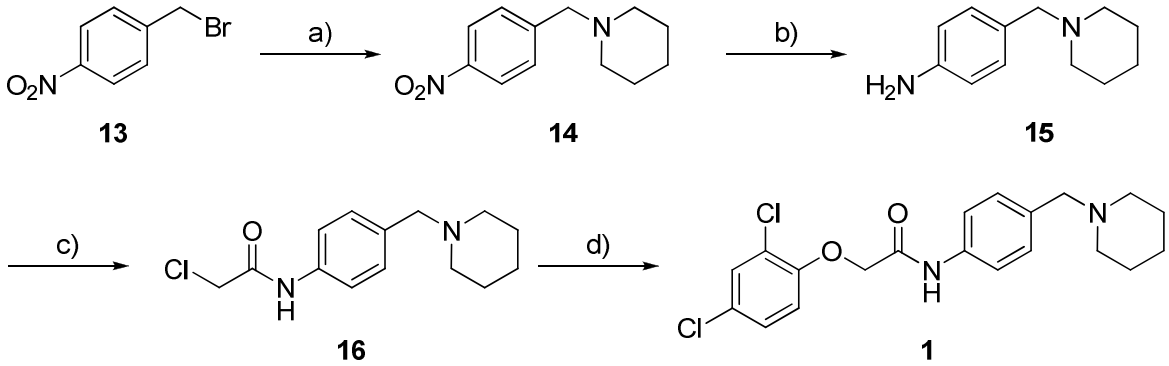


[a]Reagents and conditions: (a) piperidine (3.1 eq), THF, rt, 1h, yield 93% (b) $SnCl_2$*2 $H_2O$ (5 eq), EtOAc, rt, overnight, yield 92% (c) chloroacetyl chloride (20 eq), AcOH, NaOAc, 3h, rt, yield 92% (d) 2, 4-dichlorophenol (1.5 eq), $K_2CO_3$ (2 eq), KI (0.05 eq) DMF, rt, 16 h, yield 59%.

The potencies of the synthesized **2** and **1** were investigated by determining their $IC_{50}$ values for inhibition of *Ag*AChE1, *Aa*AChE1, *h*AChE, as well as *m*AChE and the resistance conferring mutant G122S-*Ag*AChE1 (Figure 3). Compound **2** was confirmed to be selective for the mosquito enzymes, having $S.R._{IC50}$ values of 141 and 82 for AChE1 over *h*AChE and *m*AChE,

respectively. The $IC_{50}$ values of compound **2** was 0.21 μM and 0.22 μM for inhibition of *Aa*AChE1 and *Ag*AChE, respectively. The corresponding constants for the vertebrate enzymes were 31 μM (*h*AChE) and 18 μM (*m*AChE). The $IC_{50}$ value of **2** for inhibition of the resistance conferring mutant G122S-*Ag*AChE1 was 1.3 μM, corresponding to a more than ten times selectivity over the vertebrate enzymes (Figure 3A). The non-selective binding of compound **1** to AChE1 was confirmed (Figure 3B). In fact, compound **1** had a slightly higher potency for the vertebrate enzymes (0.030 μM and 0.026 μM for *h*AChE and *m*AChE, respectively) than the mosquito enzymes (0.26 μM and 0.44 μM for *Ag*AChE1 and *Aa*AChE1, respectively). Previous measurements of the vertebrate enzymes resulted in $IC_{50}$ values for **1** that were approximately seven to twelve times higher than reported here.[33, 48] The experimental conditions in this work (*e.g.* pH, compound- and enzyme batch) were slightly different from those previously used. Importantly, all $IC_{50}$ determinations included in the present study were determined using the same conditions and are thus directly comparable. The non-selective **1** had an $IC_{50}$ value of 1.2 μM for inhibition of G122S-*Ag*AChE1, which is in agreement with previous determinations.[33]

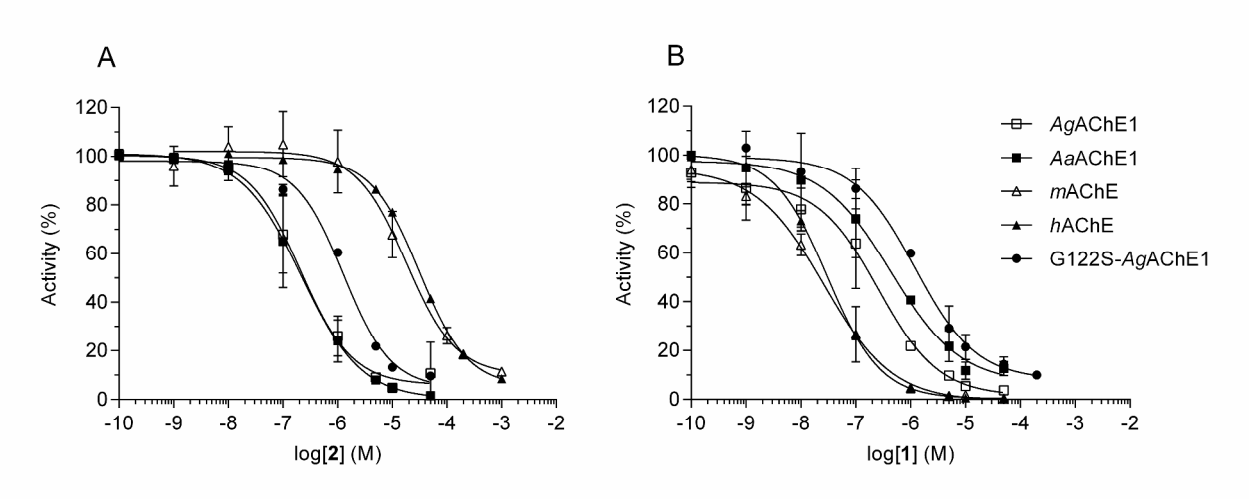


**Figure 3.** Dose-response curves for compounds **2** (A) and **1** (B). The plotted results are means ± standard deviations based on 2-3 measurements. $IC_{50}$-values against *Ag*-, *Aa*AChE1, and *h*AChE

are presented in Table 2; for compounds **2** and **1** the $IC_{50}$-values for *m*AChE were 18 (8.7-38) μM and 0.026 (0.018-0.039), respectively, and for G122S-*Ag*AChE1 1.3 (0.98-1.7) μM and 1.2 (0.77-1.9) μM, respectively.

**Structure – selectivity relationships of 2 and 1**

To investigate the structural basis for the marked differences in selectivity of **2** and **1** we studied their binding modes using a combination of X-ray crystallography and homology modeling. The 2.5 Å resolution crystal structure of **2** in complex with *m*AChE (**2**•*m*AChE, pdb code: 5FUM, see Supporting Information, Table S10, authors will release the atomic coordinates and structure factors upon article publication) illustrates the general, extended binding mode of the ligands (Figure 4). The compounds span the entire 20 Å deep active site gorge of AChE and form interactions with both Trp286 and Trp86, residues located at the rim and the base of the gorge, respectively. The binding poses in **2**•*m*AChE and the previously reported **1**•*m*AChE (pdb code: 5FOQ[51]) also involves a similar set of contacts and interactions; arene···arene interactions with indole of Trp286 are formed by the 2,4-dichlorophenyl or biphenyl arenes while their tertiary amines are located at the base of the gorge. Ligands featuring a positively charged moiety interacting with a residue deep in the catalytic site of AChE has been observed in the crystal structures of potent inhibitors.[51-54] For example, the piperidine moiety of **1** has been shown to form a strong activated CH···arene hydrogen bond with Trp86.[51] A superposition of **2**•*m*AChE and **1**•*m*AChE reveals that the piperidine fragment in **1** is located approximately 2.5 Å deeper down in the gorge than the ethylpiperazine of **2** (Figure 5A-B). This will influence the CH···arene hydrogen bond and may contribute to the lower affinity of **2** than **1**. Furthermore, it appears that steric effects could also contribute to the reduced potency of **2**, since the bulky piperidine linker is positioned in the narrow bottleneck formed by Tyr124 and Tyr337.

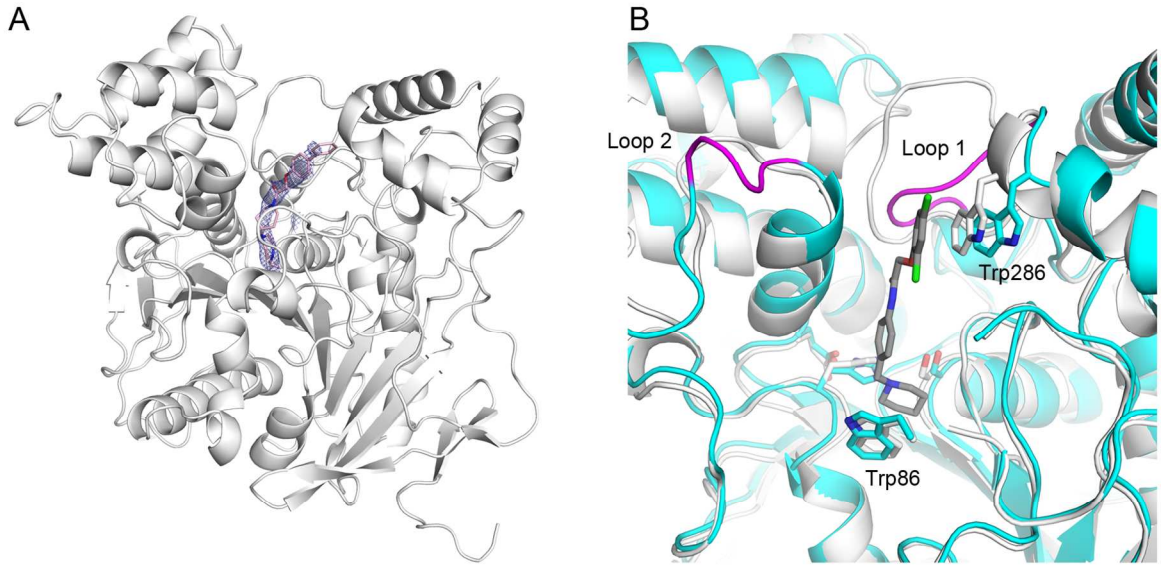


**Figure 4.** Structures of enzyme-inhibitor complexes. (A) Crystal structure of **2**•*m*AChE (pdb code: 5FUM) with compound **2** in pink and its electron density shown in blue (simulated annealing $F_o$-$F_c$ omit map at 3 σ). (B) Homology model of *Ag*AChE1 shown in cyan superimposed to **1**•*m*AChE (pdb code: 5FOQ) in white. The two loops at the entrance of the gorge responsible for the main differences between *Ag*AChE1 and *m*AChE are highlighted in magenta.

To investigate the binding of **2** and **1** to the mosquito enzymes, the corresponding structures were generated by homology modelling. The models of **1**•*Ag*AChE1 and **1**•*Aa*AChE1 were constructed using a crystal structure of *Drosophila melanogaster* AChE (*Dm*AChE) as the main template (38% and 39% sequence identity for *Ag*AChE1 and *Aa*AChE1, respectively). Note that no AChE1 crystal structure was available and that *Dm*AChE is encoded by the *ace-2* gene. The sequence identity of *Ag*AChE1 and *Aa*AChE1 was 93%, and the RMSD value based on all heavy atoms in the two homology models was low (1.2 Å). In general, the structures of *m*AChE,

*Ag*AChE1, and *Aa*AChE1 are very similar (Figure 4B); the structure of the active site is conserved and most of the amino acids in the binding site are identical. As previously reported, the most apparent differences in sequences between mosquito and vertebrate enzymes' occur in two loops located at the entrance of the gorge (Figure 4B).[30, 36] The first loop (loop 1), involving residues that define the acyl pocket, is adjacent to Trp286 and extends from Leu289 to Phe297 in the mouse and human enzymes; in the mosquito enzymes this loop is truncated by three amino acids. In addition, the residue Phe295, which in vertebrates has frequently been observed to interact with ligands,[51-52, 54-56] is replaced by a cysteine in the mosquito enzymes. The presence of a free cysteine in the active site gorge has previously been used to develop selective covalent AChE1 inhibitors.[37-40] The second loop (loop 2) extends from Gly342 to Lys348 in *m*AChE/*h*AChE; in the mosquito enzymes, loop 2 contains one additional amino acid and the proline that directs the loop's structure in *m*AChE/*h*AChE (Pro344) is missing in AChE1. While this loop may not be directly involved in ligand binding, it could affect the position of the alpha helix that includes residues such as Tyr337, Phe338, and Tyr341, all of which line the active site gorge.

The homology models showed that most of the interactions between **1** and *Ag*AChE1/*Aa*AChE1 were similar to those found in **1**•*m*AChE; the key interactions to Trp86 and Trp286 were preserved and no potentially new interactions between **1** and AChE1 were identified (see Supporting Information, Figure S22 and S23). To investigate the higher potency of **2** for *Ag*AChE1 and *Aa*AChE1 compared to *m*AChE, we rigidly modelled **2** into the homology models based on the binding pose of **1** in **1**•*m*AChE (see Experimental section for details). The modelled conformation of **2** was readily accommodated in the binding sites of *Ag*AChE1 and *Aa*AChE1 (**2** in complex with *Ag*AChE1 and *Aa*AChE are shown in Figure 5C and Supporting Information,

Figure S24A, respectively), showing that **2** can adopt a slightly different binding pose in the mosquito enzymes compared to the one observed in **2**•*m*AChE. By binding further down in the active site gorge, the piperazine moiety of **2** can thus form CH···arene hydrogen bonds with the indole of Trp286, in contrast to the suboptimal distances and geometries seen in **2**•*m*AChE. In addition, the bulky piperidine linker of **2** is well accommodated in the bottleneck region of the mosquito enzymes.

The homology model of *Ag*AChE1 including the mutation of Gly122 to serine showed that the mutation appears not to significantly affect the binding modes of compounds **1** and **2**, which is in agreement with the observed minor reduction in potency. The G122S mutation is located in the oxyanion hole near the catalytic Ser203[35] and is thereby not making contact with either of the ligands; the closest distance is approximately 5 Å between **2** and the OH of the mutated serine (see Supporting Information, Figure S24B).

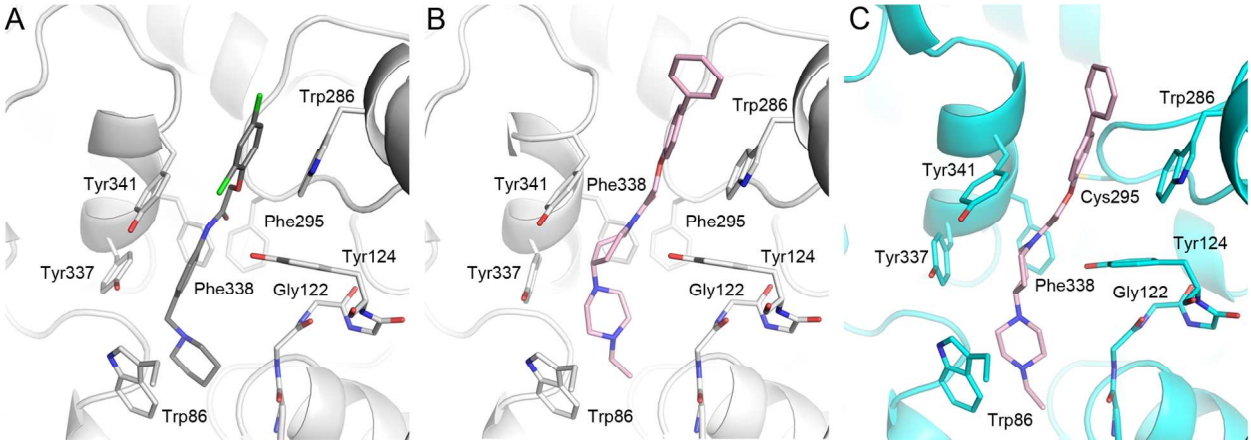


**Figure 5.** Binding poses of inhibitors in the active site gorge of *m*AChE (A-B; pdb codes: 5FOQ and 5FUM) and *Ag*AChE1 (C, homology model). The structures of *m*AChE and *Ag*AChE1 are shown in white and cyan, respectively; compounds **1** and **2** are shown in grey and pink, respectively.

## DISCUSSION

We have experimentally screened a library of 17,500 compounds for their inhibition of AChE1 from the mosquitoes *Anopheles gambiae* and *Aedes aegypti*, and the resulting hits were analyzed together with corresponding data from the previously presented HTS of the human enzyme. The screening allowed us to explore a larger chemical space of potential inhibitors compared to efforts aiming for covalent inhibitors. Covalent inhibitors target a specific amino acid in AChE1, for example Cys295[36-40] or Ser203.[20, 30, 41-46] In contrast, non-covalent inhibitors could in principle bind to any region of the protein as long as the catalytic activity is inhibited. The HTS resulted in 338 inhibitors of AChE1 that had different chemical topologies and physicochemical properties suggesting that they exploit different interaction patterns and binding poses with AChE1 compared to known covalent inhibitors, including currently used insecticides.

The AChE1- and *h*AChE hits showed similar global chemical features (e.g., molecular weight and logP), reflecting the conserved structure and function of AChEs from different species. Nevertheless, multivariate modelling based on selective hits for AChE1 and *h*AChE, respectively, indicated chemical differences between the two groups of compounds. This finding has important implications for the development of selective non-covalent inhibitors as it indicates that, in addition to the overlapping molecular properties of the two groups of hits, there also exist distinct chemical spaces that can be explored in an optimization process. From a structural point of view, the homology modeling of mosquito AChE1 suggested that the observed selectivity for the mosquito enzymes is related to structural differences of two loops at the entrance of the active site gorge. Interactions with residues in these loops have previously been proposed to confer *h*AChE over *Ag*AChE1 selectivity for non-covalent inhibitors.[30] Interestingly, the mosquito vs. vertebrate differences in the loops at the entrance of the gorge appear to influence the structure of the entire active site. This may explain the large number of selective hits despite the fact that

AChE1, *h*AChE, and *m*AChE have identical residues in the actual catalytic sites. In fact, the combination of X-ray crystallography and homology modeling of **2**, suggested that the preference for AChE1, at least partly, was due to specific interactions with Trp86, a residue more than 15 Å away from the loop regions at the entrance of the gorge. The hypothesis of differences in the catalytic sites of AChE1 and *h*AChE are further supported by previous work on covalent inhibitors targeting Ser203 where bulky inhibitors led to selectivity for *Ag*AChE1[20, 41] and our biochemical characterization of AChEs, showing that AChE1 has a higher tolerance for larger substrates compared to vertebrates enzymes.[33]

The resistance conferring mutation in G122S-*Ag*AChE1, located in the oxyanion hole of *Ag*AChE1,[35] results in a profound effect on the enzyme's ligand binding properties. So far it has proven challenging to develop covalent AChE1 inhibitors that are selective *and* active on the G122S enzyme.[42-45] Non-covalent inhibitors targeting G122S-*Ag*AChE1 have been reported, however the mosquito over human selectivity of the compounds was not presented in the study.[47] Encouragingly, both compounds **1** and **2** inhibited G122S-*Ag*AChE1. Thus, **2** combines a selectivity for the mosquito enzymes with a potency for G122S-*Ag*AChE1. This demonstrates a possibility to develop selective non-covalent inhibitors that target both the wild-type and the mutated form of AChE1, although further investigations are needed to determine the general applicability.

Our long term goal is to develop new insecticides for vector control that selectively target mosquitoes and overcome problems arising from insecticide resistance. The differential HTS generated a substantial number of hits that provide valuable chemical starting points for the insecticide development process. However, in order to be effective *in vivo* the inhibitors must not only target a relevant protein with sufficient potency, they also have to be able to penetrate the exoskeleton and survive the metabolism of mosquitoes. New AChE1 inhibitors have shown

insecticidal activity on mosquitoes,[41-43, 45, 47] although a generally much lower *in vivo* compared to *in vitro* potency of these inhibitors highlights the importance of the pharmacokinetic as well as the pharmacodynamic properties. Furthermore, factors such as human safety, cost of goods, and environmental sustainability also need to be adequately addressed. During such a multiobjective optimization process (*cf.* drug discovery process) many compounds will likely fail, making multiple compound classes highly desirable in order to increase the prospect of success.

## CONCLUSIONS

To discover new inhibitors of *Ag*AChE1 and *Aa*AChE1, we successfully adapted the Ellman assay to a format where we could screen 17,500 compounds. The assay proved to be robust and 338 hits of *Ag*AChE1 and *Aa*AChE1 were identified. The dose-response analysis generally agreed well with the screening data, confirming the quality of the screen. Importantly, several inhibitors were identified with sub-micromolar to low micromolar potency for the mosquito enzymes.

Considering the evolutionary conserved structure and function of AChE, a surprisingly large fraction of the hits was selective for AChE1 over the human enzyme. Chemical differences could be identified between the two sets of hits, although their overall global properties were similar. The chemical cluster tree revealed that structurally related hits were prone to have similar selectivity profiles, although inhibitors with subtle differences in their chemical structures could still have different selectivity. The sub-micromolar inhibitors **2** and **1** were synthesized and their different selectivity profiles were confirmed. They were also shown to be potent inhibitors of the resistance conferring mutant G122S-*Ag*AChE1. The structure-selectivity relationship of **2** and **1** for the mosquito and mouse enzymes could be established by X-ray crystallography and homology modelling. Two loops at the entrance of the active site gorge that differ between the

enzymes appear to cause differences in the entire active site explaining the selectivity profiles of **2** and **1**. The structural analysis can be extended to the complete set of hits as the proposed differences in the active site gorge may explain the large number of selective inhibitors.

Multiple compound classes will be needed in the development process of new insecticides for vector control to combat mosquito-borne diseases. Non-covalent inhibitors of AChE1, such as the ones presented here, provide valuable starting points, and are complementary to existing and new covalent inhibitors since they are chemically different and have different interaction characteristics with the enzymes.

## EXPERIMENTAL SECTION

### High throughput screening

The collection of 17,500 compounds used in this work is maintained as part of the screening platform of the Laboratories for Chemical Biology, Umeå (LCBU).[57] Recombinant AChE1 enzymes from the mosquitoes *Anopheles gambiae* and *Aegypti aegypti* were expressed in insect *Sf-9* cells using a baculovirus expression system, as described previously.[33] The screen was performed using secreted non-purified proteins in growth medium, and enzymatic activity was measured using the Ellman assay[49] adapted to a 96-well format. Assays were performed in a final volume of 200 µL of 0.1 M phosphate buffer (pH 7.4) containing 0.2 mM 5,5′-dithiobis(2-nitrobenzoic acid) and 1 mM acetylthiocholine iodide. Stock solutions of the compounds in DMSO (5 mM) were transferred to the assay plates using a Biomek NX$^P$ Laboratory Automation Workstation (Beckman Coulter, Inc.) to give a final compound concentration of 50 µM. Each plate contained 80 compounds in DMSO, eight positive controls (without compound) and eight negative controls (without compound and substrate). The enzymatic reaction was measured by monitoring changes in the absorbance of individual wells at 412 nM over 60 s in an Infinite

M200 Microplate reader (Tecan Group Ltd., Männedorf, Switzerland). The average slope (typically 0.40±0.03 and 0.53±0.03 dA/min for *Ag*AChE1 and *Aa*AChE1, respectively) determined for the eight positive controls on each plate was taken to represent 100% activity and the activity observed in the sample wells were quantified in relation to this value. Compounds that reduced the measured activity by at least three times the standard deviation of the mean for the 17,500 compounds were scored as hits.

**Assay stability and robustness**

A reference plate was analysed after every 10-20$^{th}$ plate of samples to monitor the stability of the screening assay; in total, 27 reference plates were run while screening with *Ag*AChE1 and 12 with *Aa*AChE1. Each plate contained eight compounds, with eight evenly spaced replicates of each compound. Five of the compounds had $IC_{50}$ values ranging from 0.05 to 100 μM for both enzymes; the other three compounds were inactive up to 1000 μM and used as positive controls (see Supporting Information, Figure S4 and Table S2). The Z'-factor[50] was calculated for each reference plate using the following expression: $Z'=1 - ((3SD_{c+} + 3SD_{c-})/|\mu_{c+} - \mu_{c-}|)$. In these calculations, data for eserine and AL045 were used as negative and positive controls, respectively (see Supporting Information, Figures S4-S7 and Table S2).

**Selection of hits for $IC_{50}$ determinations**

The hits were divided into groups based on their activity in the HTS (if a hit was classified into different groups for the two AChE1 enzymes, it was assigned to a group based on its highest observed inhibitory potency). The first group consisted of hits that reduced the enzymatic activity of AChE1 by ≥ 70%; a representative subset of compounds with diverse structural and physicochemical features was manually selected from this group and designated set A. Similarly, another set of compounds was selected from the group of compounds that achieved 31-69% inhibition in the HTS (set B), and a third set (set C) was selected from the group of compounds

that were not scored as hits but had similar structural and physicochemical properties to the compounds in sets A and B. Finally, a fourth set of compounds were manually selected from the hits whose inhibitory potency towards *Ag*- and *Aa*AChE1 differed by ≥ 30%. For more details, see the Supporting Information, Tables S4 and S5 and Figures S8-S17.

**$IC_{50}$ determinations**

Dose-response experiments based on the Ellman assay[49] were performed on hit compounds that were selected for follow up evaluation. The enzymes used in these experiments were the recombinant variants of AChE1,[33] *h*AChE,[58] and *m*AChE.[59] The compounds were purchased from Chem-Bridge (San Diego, CA) or accessed via the LCBU,[57] except **2** and **1** which were synthesized (see Synthesis section below). The compounds' structures were confirmed by $^1$H NMR and $^1$H COSY, and their purity was confirmed to be ≥ 95% by LC-MS (detection at 254 nm; see the Synthesis section below and Supporting Information, pages S32-S36). Stock solutions of the compounds were prepared from solid material in DMSO at a concentration of 100 mM and working dilutions thereof were prepared in either 0.1 M sodium phosphate buffer (pH 7.4) or MilliQ water. Compound solutions of at least eight different concentrations up to a maximum of 1 mM were used. The assay was performed under the same conditions as described above for the HTS, with the difference that it was handled manually, only eight wells were monitored at a time, and the assay was run at 30 °C. The average enzymatic activity determined for the eight wells of un-inhibited enzyme on the plate was defined as 100% activity and the activity observed in the inhibited wells was quantified in relation to this value. $IC_{50}$ values were calculated using non-linear regression (curve fitting) in GraphPad Prism[60] and the log [inhibitor] vs. response variable slope equation was fitted using four parameters. In certain cases, three-parameter analyses were used instead. The $IC_{50}$ values presented in Table 1 were determined independently twice using 1-2 replicates on each occasion for all compounds other than **9**, which

exhibited poor solubility. The complete HTS and follow up data of **1-10** and the remaining compounds in set A-D, whose activity was assessed once using 1-2 replicates, is presented in Supporting Information, Table S6.

**Selectivity profiles**

Based on the observations from the dose-response evaluations, the following criteria were established in order to delineate selectivity profiles for the hits based on their HTS data. Potentially AChE1 selective hits were required to i) be identified as hits against at least one mosquito enzyme, ii) not be identified as a hit against *h*AChE, and iii) inhibit both *Ag*AChE1 and *Aa*AChE1 at least five times more effectively than *h*AChE in the HTSs. Potentially *h*AChE selective compounds were identified as hits that i) were identified as *h*AChE hits, ii) were not identified as *Ag*AChE1 or *Aa*AChE1 hits, and iii) inhibited *h*AChE at least five times more effectively than both *Ag*AChE1 and *Aa*AChE1 in the HTSs. Non-selective hits were required to be identified as hits of AChE1 *and h*AChE. All remaining hits were classified as miscellaneous.

**Discriminant analysis of AChE1- and *h*AChE selective hits**

Prior to calculation of physicochemical 2D-descriptors and MACCS fingerprints, the neutral chemical structures of the hit compounds were prepared by removing small fragments (i.e. metals or groups in salts), adding explicit hydrogens, and scaling of bonds using the 'wash' option in MOE.[61] A regression discriminant analysis was made based on all the AChE1 selective compounds that were scored as hits against both *Ag*AChE1 and *Aa*AChE1 (83 hits) and the *h*AChE selective compounds (74 hits) according to the criteria in the section above. The physicochemical properties of the hits were described by 85 2D-descriptors that were calculated using the MOE software.[61] Orthogonal partial least squares-discriminant analysis (OPLS-DA),[62] a supervised multivariate classification method, was used to identify physicochemical properties that could discriminate between the AChE1- and *h*AChE selective hits. The data were mean-

centered and scaled to unit variance before an OPLS-DA model was calculated using the SIMCA-P+ software.[63] The model was iteratively refined by excluding 2D descriptors with small influence on the model (i.e. weighted sum of squares of the w* weights less than 0.5). The number of significant model components was determined by cross-validation. The results are presented in the Supporting Information, Tables S7 and S8, and Figure S18. The significance of model variables (2D descriptors) for discriminating between AChE1- and *h*AChE hits was confirmed by Student's T-test ($\alpha = 0.05$) (see Supporting Information, Table S8 and Figure S18).

**Chemical structural tree**

The chemical structures of the AChE1- and *h*AChE hits were described in terms of 166 MACCS fingerprints[64] using the MOE software.[61] A matrix of Soergel distances[65] between the hits was calculated, where the Soergel distance between two hits A and B was calculated as $D_{AB}$ = (a+b - 2*c) / (a + b -c). Here, *a* is the number of bits set to "1" in the MACCS fingerprint vector of hit A, *b* is the number of bits set to "1" in the fingerprint vector of hit B, and *c* is the number of bits set to "1" in the fingerprint vectors of both hit A *and* hit B. The hits were clustered on the basis of their Soergel distances using the Neighbour-Joining method[66] in the PHYLIP software[67] after randomizing their order. The clustering was visualized in the form of an unrooted tree with the angle of the arc set to 360 degrees; the tree's branch lengths correspond to the Soergel distances between the hits. A short distance between two hits means that they are chemically similar. The selectivity profile of each hit (which could be potentially AChE1 selective, non-selective, or potentially *h*AChE selective) was mapped onto the tree.

**Synthesis**

*General.* All reactions were carried out under inert atmosphere ($N_2$) unless otherwise stated. THF and DMF were dried in a solvent drying system and freshly collected prior to reaction (THF was passed through neutral alumina, DMF was passed thorough activated molecular sieves

followed by an isocyanate scrubber). All microwave reactions were carried out in a monomode reactor using Smith process vials sealed with a Teflon septum and an aluminum crimp top. The temperature was measured with an IR sensor and reaction times refer to the irradiation time at the target temperature. Reactions were monitored using TLC (silica gel matrix, layer thickness 200 µm, particle size 25 µm) with UV-detection (254 nm) or developed using $KMnO_4$ solution. Flash column chromatography (eluents given in brackets) was performed on normal phase silica gel (Merck, 60 Å, 40-63 µm). $^{1}H$ and $^{13}C$ NMR spectra were recorded on a Bruker DRX-400 instrument at 298 K in $CDCl_3$ using residual $CHCl_3$ ($\delta_H$ = 7.26 ppm) or $CDCl_3$ ($\delta_C$ = 77.0 ppm) as an internal standard, $(CD_3)_2SO$ using residual $(CD_3)(CD_2H)SO$ ($\delta_H$ = 2.50 ppm) or $(CD_3)_2SO$ ($\delta_C$ = 40.0 ppm) as an internal standard, or $CD_3OD$ using residual $CD_2HOD$ ($\delta_H$ = 3.31 ppm) or $CD_3OD$ ($\delta_C$ = 49.0 ppm) as an internal standard, or $D_2O$ using traces of $CH_3OH$ ($\delta_H$ = 3.34 ppm) or $CH_3OH$ ($\delta_C$ = 49.50 ppm) as an internal standard (Supporting Information, pages S32-S42). LC-MS analyses were performed on a Waters LC system using a Xterra MS C18 18.5 µm 4.6x50 mm column and an acetonitrile:water eluent system containing 0.2% formic acid. Eluting compounds were detected by monitoring the eluent's absorption at 254 nm and mass spectrometry was performed in positive ion mode using a Waters micromass ZG 2000 electrospray instrument. Analytical HPLC was performed using a Nexera UHPLC system (Shimadzu, US) connected to a diode array detector (SPP M20A). Samples were analyzed using a Nucleodur C18 HTec column (EC 150 × 4.6, 5 µm, Macherey-Nagel) with a flow rate of 1 ml/min. Aliquots of 2 µl of each sample were injected, and detection was performed at 254 nm. The mobile phase was composed of solvent A ($H_2O$ with 0.1% TFA) and solvent B (acetonitrile with 0.1% TFA). The binary gradient profile was as follows with solvent B as the reference: 0–1.5 min, 10% B; 1.5–11.5 min, 10–100% B; 11.5–26.5 min, 100% B; 26.5–27 min, 100–10% B; 27–30.5 min, 10% B. Before first injection, the column was equilibrated at 10% B for 1.5 min.

The synthesized compounds used in the biological evaluations exhibited ≥ 95% purity by the HPLC analysis.

**2-(2,4-Dichlorophenoxy)-N-[4-(piperidin-1-ylmethyl)phenyl]acetamide (1)**. $K_2CO_3$ (142 mg, 1.03 mmol) and KI (4 mg, 0.03 mmol) were added to **16** (137 mg, 0.51 mmol) and 2,4-dichlorophenol (126 mg, 0.77 mmol) in dry DMF (4 ml) at rt while stirring. Stirring was continued at rt for 16 h before the reaction mixture was poured into EtOAc and washed three times with $NaHCO_3$ (sat), followed by water and brine. The organic layer was dried over $Na_2SO_4$, filtered, and concentrated under reduced pressure to give an off-white solid. Recrystallization from EtOH:heptane gave **1** (120 mg, 59% yield) as white needles. $^1$H NMR (400 MHz, $CDCl_3$) δ 8.52 (br s, 1H), 7.52 (d, $J$ = 8.5 Hz, 2H), 7.41 (d, $J$ = 2.5 Hz, 1H), 7.29 (d, $J$ = 8.5 Hz, 2H), 7.22 (dd, $J_1$ = 2.5 Hz, $J_2$ = 8.8 Hz, 1H), 6.86 (d, $J$ = 8.8 Hz, 1H), 4.58 (s, 2H), 3.43 (s, 2H), 2.38-2.30 (m, 4H), 1.58-1.52 (m, 4H), 1.44-1.38 (m, 2H). $^{13}$C NMR (100 MHz, $CDCl_3$) δ 164.8, 151.3, 135.4, 135.4, 130.1, 129.8 (2C), 128.0, 127.6, 123.7, 119.6 (2C). 114.8, 68.3, 63.2, 54.3 (2C), 25.9 (2C), 24.3.

**2-([1,1'-Biphenyl]-4-yloxy)-1-[4-(4-ethyl-1-piperazinyl)-1-piperidinyl]-ethanone hydrochloride (2)**. TBTU (42 mg, 0.13 mmol) and 1-ethyl-4-piperidin-4-yl-piperazine (26 mg, 0.13 mmol) were added to **12** (25 mg, 0.11 mmol) in dry DMF (1 ml), at rt while stirring. TEA (46 µl, 0.33 mmol) was added dropwise followed by an additional 1 ml of dry DMF. The cloudy reaction mixture was stirred at rt for five days. Upon addition of $NaHCO_3$ (sat.) to the reaction mixture a white precipitate was formed that dissolved upon addition of $H_2O$. The resulting aqueous layer was extracted three times with EtOAc, after which the combined organic layers were washed three times with brine, dried over $Na_2SO_4$, filtered, and concentrated. The resulting crude material was cooled on ice, treated with half-saturated HCl in $CH_2Cl_2$ (5 ml) and stirred for 20 h while slowly being allowed to attain rt. The solvent was then removed under reduced

pressure and the resulting crude product was recrystallized from MeOH:EtOAc to give a white solid that was filtered off and washed with a small amount of EtOAc. The mother liquor was concentrated and the resulting solid triturated with EtOAc before the recrystallization was repeated once to give 24 mg (47% yield) of **2** as a white solid. $^{1}$H NMR (400 MHz, $D_2O$) δ 7.62-7.58 (m, 4H), 7.48-7.44 (m, 2H), 7.38-7.34 (m, 1H), 6.99 (d, *J* = 8.7 Hz, 2H), 4.82 (d, *J* = 15.1 Hz, 1H), 4.71 (d, *J* = 15.1 Hz, 1H), 4.51 (d, *J* = 13.6 Hz, 1H), 3.95 (d, *J* = 13.6 Hz, 1H), 3.75-3.44 (m, 9H), 3.32 (q, $J_1$ = 7.3 Hz, $J_2$ = 14.7 Hz, 2H), 3.12 (t, *J* = 12.8 Hz, 1H), 2.70 (t, *J* = 12.8 Hz, 1H), 2.19 (m, d, *J* = 11.5 Hz, 2H), 1.69-1.49 (m, 2H), 1.34 (t, *J* = 7.3 Hz, 3H). $^{13}$C NMR (100 MHz, $D_2O$) δ 168.9, 157.6, 140.3, 134.6, 129.8 (2C), 128.7 (2C), 128.0, 127.1 (2C), 115.8 (2C), 66.1, 63.5, 53.0, 49.2 (2C), 46.6 (2C), 43.5, 41.2, 27.1, 26.5, 9.2.

**(Biphenyl-4-yloxy)-acetic acid (12)**. Chloroacetic acid (278 mg, 2.94 mmol) followed by NaOH (s) (165 mg, 4.11mmol) were added to 4-phenylphenol **11** (100 mg, 1.76 mmol) in MeOH (6 ml) at rt while stirring. The reaction mixture was then heated and stirred at reflux for 24 h, allowed to cool to rt, and acidified by adding 1M HCl. The resulting solution was concentrated under reduced pressure to remove MeOH and the formed white precipitate was filtered off and washed with small amounts of water to yield **12** (39 mg, 29% yield) as a white solid. $^{1}$H NMR (400 MHz, $CD_3OD$) δ 7.56 (m, 4H), 7.41-7.37 (m, 2H), 7.27 (t, *J* = 7.4 Hz, 1H), 7.01 (d, *J* = 8.7 Hz, 2H), 4.69 (s, 2H). $^{13}$C NMR (100 MHz, $CD_3OD$) δ 172.7, 159.0, 142.0, 135.8, 129.8 (2C), 129.0 (2C), 127.8, 127.6 (2C), 116.0 (2C), 65.9.

**1-(4-Nitrobenzyl)piperidine (14)**. Piperidine (750 µl, 7.58 mmol) followed by dry THF (3 ml) were added to 4-nitrobenzyl bromide **13** (523 mg, 2.42 mmol) in dry THF (3 ml) at rt while stirring. A precipitate was immediately formed and the reaction mixture was allowed to stir at rt for 1 h before being diluted with $Et_2O$. The resulting mixture was washed three times with 1 M NaOH and then extracted three times with 1 M HCl. The combined aqueous layers were made

basic with 2 M NaOH and extracted three times with $Et_2O$. The combined organic layers were dried over $Na_2SO_4$, filtered, and concentrated under reduced pressure to give **14** (494 mg, 93% yield) as a yellow oil. $^1$H NMR (400 MHz, $CDCl_3$) δ 8.05 (d, *J* = 8.8 Hz, 2H), 7.42 (d, *J* = 8.8 Hz, 2H), 3.45 (s, 2H), 2.34-2.22 (m, 4H), 1.52-1.46 (m, 4H), 1.38-1.33 (m, 2H). $^{13}$C NMR (100 MHz, $CDCl_3$) δ 146.9, 146.6, 129.1 (2C), 123.0 (2C), 62.6, 54.3 (2C), 25.7 (2C), 23.9.

**4-(Piperidylmethyl)aniline (15)**. $SnCl_2$ * 2 $H_2O$ (2.53 g, 11.21 mmol) was added to **14** (494 mg, 2.24 mmol) in EtOAc (20 ml) at rt while stirring. The reaction mixture was stirred overnight, filtered through a glass wool plug into $NaHCO_3$, and the resulting mixture was extracted three times with EtOAc. The combined organic layers were dried over $Na_2SO_4$, filtered, and concentrated to give **15** (112 mg, 26% yield). The yield was increased by thorough washing of the glass wool plug with EtOAc, followed by drying over $Na_2SO_4$, filtration and evaporation of the solvent, to give **15** (total amount 393 mg, 92% yield) as a cream colored solid which was used without further purification. $^1$H NMR (400 MHz, $CDCl_3$) δ 7.08 (d, *J* = 8.4 Hz, 2H), 6.62 (d, *J* = 8.4 Hz, 2H), 3.64 (br s, 2H), 3.37 (s, 2H), 2.48-2.27 (m, 4H), 1.59-1.53 (m, 4H), 1.44-1.41 (m, 2H). $^{13}$C NMR (100 MHz, $CDCl_3$) δ 145.1, 130.3 (2C), 128.0, 114.6 (2C), 63.3, 54.1 (2C), 25.8 (2C), 24.3.

**2-Chloro-N-(4-piperidin-1-ylmethyl-phenyl)-acetamide (16)**. Half-saturated NaOAc (aq.) (5 ml) followed by chloroacetylchloride (0.82 ml, 10.3 mmol) were added to aniline **15** (393 mg, 2.07 mmol) in AcOH (15 ml) at rt while stirring. After stirring at rt for 3 h, another 0.82 ml of chloroacetylchloride was added and a milky precipitate was formed. Half-saturated NaOAc (aq.) was added until the precipitate dissolved, and an additional 1.6 ml of chloroacetylchloride was added. After stirring for 15 minutes, the solution was made basic by adding $Na_2CO_3$ (s) and extracted three times with EtOAc. The combined organic layers were washed with brine, dried over $Na_2SO_4$, filtered, and concentrated under reduced pressure to give **16** (509 mg, 92% yield)

as an off-white solid. $^{1}$H NMR (400 MHz, $CDCl_3$) δ 8.23 (br s, 1H), 7.47 (d, $J$ = 8.4 Hz, 2H), 7.30 (d, $J$ = 8.4 Hz, 2H), 4.17 (s, 2H), 3.44 (s, 2H), 2.39-2.30 (m, 4H), 1.58-1.53 (m, 4H), 1.44-1.39 (m, 2H). $^{13}$C NMR (100 MHz, $CDCl_3$) δ 163.7, 135.7, 135.3, 129.8 (2C), 119.9 (2C), 63.2, 54.4 (2C), 42.8, 25.9 (2C), 24.3.

**Generation, collection and refinement of crystal structures**

*m*AChE was crystallized as previously described.[59] Grains of the ligand were added to a soaking solution consisting of 30% (v/v) polyethylene glycol 750 monomethylether in 100 mM HEPES buffer, pH 7.0 until saturation was reached. The soaking solution was then added to a crystal of *m*AChE. Soaking was performed over a time-frame of five minutes and the crystal was incubated for an additional five minutes prior to flash-freezing in liquid nitrogen. X-ray diffraction data were collected at the MAX-lab synchrotron (Lund, Sweden) using beam lines I911-2 and I911-3, which were equipped with MAR Research CCD detectors. 180 images were collected using an oscillation angle of 1.0° per exposure. The intensity data were indexed and integrated using XDS[68] and scaled using Scala[69]. The structure of **2**•*m*AChE was determined using rigid-body refinement starting with a modified *apo* structure of *m*AChE (pdb code: 1J06[53]). Further crystallographic refinement was performed using the Phenix software suite.[70] The coordinates of **2** were modelled in the binding site of *m*AChE according to the initial $2|F_o|-|F_c|$ and $|F_o|-|F_c|$ electron density maps. Several rounds of refinement were performed, alternating with manual rebuilding of the model after visualizing the $2|F_o|-|F_c|$ and $|F_o|-|F_c|$ electron density maps using COOT.[71] Simulated annealing omit maps, starting from the model where the coordinates for **2** were omitted, were used to confirm the presence of the ligand and to generate Figure 4A. While the electron density maps clearly define the binding pose of **2**, it was not possible to assign the conformations of the piperidine-piperazine ring system and the electron density of the distant 1'-phenyl ring was not fully defined at a contour level of 1 σ. Furthermore,

residual positive difference density around the side chain of Asp74 could not be modelled. The figures were constructed using PyMol[72] (see Supporting Information, Table S10).

**Multiple sequence alignment**

The amino acid sequences of *Ag*AChE1[73] (accession no: XP_321792; UNIPROT code: ACES_ANOGA ) and *Aa*AChE1[29] (accession no: ABN09910) were aligned to *Tc*AChE (pdb code 1EA5[74]; UNIPROT code: ACES_TORCA), *h*AChE (pdb code 4EY4[56]; UNIPROT code: ACES_HUMAN), *m*AChE (pdb code 1J06[53]; UNIPROT code: ACES_MOUSE), and *Dm*AChE, pdb code 1QO9[34]; UNIPROT code: ACES_DROME) using ClustalW[75] and MOE.[61] The resulting multiple alignments were inspected and the alignment of loop 1 in *Aa*AChE1 was manually adjusted according to the alignment of loop 1 in *Ag*AChE1 to give the final alignment (see Supporting Information, pages S43-S44).

**Template preparation**

Two templates, **1**•*m*AChE and **1**•*Dm*AChE, were selected and prepared as follows (see Supporting information, Figure S20). The coordinates of **1**•*m*AChE, were obtained from its crystal structure (pdb code 5FOQ, chain A, 2.3 Å resolution).[51] For the second template, **1**•*Dm*AChE, the coordinates were generated by modelling of **1** into the active site of the crystalized structure of *Dm*AChE (pdb code 1DX4, chain A, 2.7 Å resolution)[34] using the coordinates from **1**•*m*AChE (pdb code 5FOQ)[51] to give template complex **1**•*Dm*AChE. Using the MOE software,[76] ionization states were optimized and hydrogens were added to the generated template complexes using the generalized Born/volume integral implicit solvent model (cutoff at 15 Å at 300 K) at pH 7 with a salt concentration of 0.1 M (assuming a dielectric constant of 1 for solutes and 80 for the solvent) and the van der Waals functional form 800R3.[77]

## Homology modeling

Homology modeling of *Ag*AChE1 and *Aa*AChE1 were performed in parallel using the homology model application implemented in MOE[76] with the Amber 99 force field[78-79] and the Reaction field solvation model. The residues of the **1**•*Dm*AChE template complex were used for modelling with the exception of the residues 102-112, 487-499, and 512-520 (*h*AChE numbering), for which the corresponding residues of **1**•*m*AChE (pdb code 5FOQ[51]) were used (see Supporting Information, Figure S20). The homology modelling was carried out in four steps. First, heavy atom coordinates of the backbone were copied from the template, and for identical amino acids in the modelled sequence and the template, also the heavy atom coordinates of the side chains were copied to give an initial partial geometry. In the second step, coordinates were extracted from a library of fragments derived from high-resolution structures in the Protein Data Bank[80] to fill in gaps in the initial model, e.g. missing coordinates resulting from insertions and deletions. Possible loop conformations were evaluated using a contact energy function, which also include already modeled residues and ligand **1**, and a Boltzmann-weighted selection of loops was made. Potential side chain conformations of the loops were sampled 5 times at 300 K using a rotamer library and selected to give an optimal packing. Using molecular mechanics, tethered minimizations were run to relieve steric strains. The homology modeling procedure was repeated 10 times to give 50 intermediate models in total. Finally, the model with the lowest electrostatic solvation energy as computed with the Generalized Born/Volume Integral method[81] was selected and ionization states and proton placements were optimized as described for the template preparation to give the final homology model.

The obtained models were manually inspected and incorrect hybridization states and chiralities were corrected. The homology models were prepared by assigning bond orders and creating

disulfide bonds in Maestro,[82] before a constrained energy minimization was performed of each model in presence of ligand **1** using the Polak-Ribiere Conjugate Gradient method[83] with the OPLS2005 force field[84] and Generalized-Born/Surface-Area solvation model (dielectric constant of 80) in Macromodel.[85] Partial charges were calculated using the OPLS2005 force field[84] and non-bonded interactions were considered within distance of 8.0, 12.0, and 4.0 Å for van der Waals, electrostatic, and hydrogen bond interactions, respectively. The positions of all heavy atoms were allowed to move +/- 0.2 Å from their initial positions before facing a resistive force of 100 kJ/mol Å$^2$, and the gradient convergence threshold was set to 0.05.

Deviating phi and psi angles according to Ramachandran plots were adjusted by an iterative cycle of constrained energy minimizations as described above with the following exceptions: deviating residues and nearest residue neighbors could move freely while all other heavy atoms were allowed to move +/- 0.1 Å before facing a resistive force of 100 kJ/mol Å$^2$. Finally, the $\chi_1$ ($C_\alpha$-$C_\beta$) and $\chi_2$ ($C_\beta$-$C_1$) dihedral angles for the side chain of Tyr337 were adjusted according to those observed in the ligand-*m*AChE complex with pdb code 4ARB[55] (Supporting Information, Figure S21) followed by additional rounds of energy minimization as described above. The final models were evaluated using PROCHECK[86] (Supporting Information, Table S9).

The homology model of G122S-*Ag*AChE1 was constructed from the homology model of *Ag*AChE1 by *in silico* mutation of Gly122 to a serine using the MOE software.[76] The resulting model was then subjected to two consecutive constrained energy minimizations using Macromodel[85] as described above. In the first minimization, the Ser122 and all residues within 3 Å of this mutated residue were allowed to move freely while all other heavy atoms were allowed to move +/- 0.1 Å from their initial positions before facing a resistive force of 100 kJ/mol Å$^2$. In the second minimization, all heavy atoms were allowed to move +/- 0.1 Å from their initial positions before facing a resistive force of 100 kJ/mol Å$^2$.

**Modelling of 2 in the active site of AChE1**

Partial charges were calculated using the MMFF94x force field[87] in MOE[76] and stochastically generated conformations of **2** were aligned to **1** in *m*AChE (pdb code 5FOQ[51]) using the flexible alignment tool implemented in MOE.[88] Alignments were evaluated both in terms of the internal energy of the ligand using the MMFF94x force field,[87] and the similarity of the conformations based on molecular features such as hydrogen bond acceptors and donors, size, and hydrophobic moieties. This yielded one conformation of **2**, which was manually docked into the active site of the homology models of *Ag*AChE1, *Aa*AChE1, and G122S-*Ag*AChE1. The models were subjected to a constrained energy minimization using Macromodel[89] as described above with all of the heavy atoms being allowed to move no more than +/- 0.2 Å from their initial positions before facing a resistive force of 100 kJ/mol $Å^2$.

ASSOCIATED CONTENT

**Supporting Information**

Data and statistics of the HTS campaigns against *Ag*AChE1 and *Aa*AChE1 including reference plate data and analysis; analysis of the physicochemical properties of the hits and the selection of compounds for $IC_{50}$ determinations; complete inhibition results for all re-tested compounds and dose-response curves for compounds **3**-**10**; compound characterization including $^1H$ NMR and $^{13}C$ NMR spectra; supplementary information regarding X-ray crystallography and homology modelling including multiple sequence alignments, template selection, **1** and **2** modelled into the active sites of *Ag*AChE1 and *Aa*AChE1, and data collection and refinement statistics for 5FUM

Molecular formula strings

## PDB ID Codes

Authors will release the atomic coordinates and experimental data upon article publication of the crystal structure of **2**•*m*AChE (pdb code: 5FUM).

## AUTHOR INFORMATION

### Corresponding Author

* Corresponding authors

E-mail address: anna.linusson@umu.se; fredrik.ekstrom@foi.se

Telephone number: Anna Linusson +46(0)907866890, Fredrik Ekström +46(0)90106815

### Author Contributions

The manuscript was written through contributions of all authors. All authors have given approval to the final version of the manuscript. $ These authors contributed equally.

### Funding Sources

The research was funded by the Swedish Research Council (grant number: 2014-2636).

## ACKNOWLEDGMENT

We thank staff at the LCBU for valuable support during the screening campaign, and Dr. Nina Forsgren and Dr. Tomas Kindahl for contributions to the biochemical evaluations and organic syntheses. We are also grateful for excellent technical support at the MAXlab beam lines.

## ABBREVIATIONS

AChE, acetylcholinesterase, *Aa*AChE1, *Aedes aegypti* acetylcholinesterase1; *Ag*AChE1, *Anopheles gambiae* acetylcholinesterase1; *Dm*AChE, *Drosophila melanogaster*

acetylcholinesterase; *h*AChE, *Homo sapiens* acetylcholinesterase; IRS, indoor residual spraying; ITN, insecticide treated bed nets; *m*AChE*, Mus musculus* acetylcholinesterase; OPLS-DA, orthogonal partial least squares-discriminant analysis; sat., saturated; TBTU, O-(Benzotriazol-1-yl)-N,N,N′,N′-tetramethyluronium tetrafluoroborate; *Tc*AChE, *Torpedo californica* acetylcholinesterase; TEA, triethylamine

REFERENCES

1. Lindgren, E.; Andersson, Y.; Suk, J. E.; Sudre, B.; Semenza, J. C. Public health. Monitoring EU emerging infectious disease risk due to climate change. *Science* **2012**, *336*, 418-419.

2. World Health Organization, A global brief on vector-borne diseases. World Health Organization, Geneva, 2014, (WHO/DCO/WHD/2014.1).

3. World Health Organization, DENGUE: Guidelines for diagnosis, treatment, prevention and control. New edition. World Health Organization, Geneva, 2009, (WHO/HTM/NTD/DEN/2009.1).

4. Bhatt, S.; Gething, P. W.; Brady, O. J.; Messina, J. P.; Farlow, A. W.; Moyes, C. L.; Drake, J. M.; Brownstein, J. S.; Hoen, A. G.; Sankoh, O.; Myers, M. F.; George, D. B.; Jaenisch, T.; Wint, G. R. W.; Simmons, C. P.; Scott, T. W.; Farrar, J. J.; Hay, S. I. The global distribution and burden of dengue. *Nature* **2013**, *496*, 504-507.

5. World Health Organization, World Malaria Report 2015. World Health Organization, Geneva, 2015.

6. Bhatt, S.; Weiss, D. J.; Cameron, E.; Bisanzio, D.; Mappin, B.; Dalrymple, U.; Battle, K. E.; Moyes, C. L.; Henry, A.; Eckhoff, P. A.; Wenger, E. A.; Briet, O.; Penny, M. A.; Smith, T. A.; Bennett, A.; Yukich, J.; Eisele, T. P.; Griffin, J. T.; Fergus, C. A.; Lynch, M.; Lindgren, F.; Cohen, J. M.; Murray, C. L. J.; Smith, D. L.; Hay, S. I.; Cibulskis, R. E.; Gething, P. W. The effect of malaria control on *Plasmodium falciparum* in Africa between 2000 and 2015. *Nature* **2015**, *526*, 207-211.

7. Casida, J. E.; Quistad, G. B. Golden age of insecticide research: Past, present, or future? *Annu. Rev. Entomol.* **1998**, *43*, 1-16.

8. Casida, J. E.; Durkin, K. A. Neuroactive insecticides: Targets, selectivity, resistance, and secondary effects. *Annu. Rev. Entomol.* **2013**, *58*, 99-117.

9. Johnson, R. M. Honey bee toxicology. *Annu. Rev. Entomol.* **2015**, *60*, 415-434.

10. Hemingway, J.; Hawkes, N. J.; McCarroll, L.; Ranson, H. The molecular basis of insecticide resistance in mosquitoes. *Insect Biochem. Mol. Biol.* **2004**, *34*, 653-665.

11. Rivero, A.; Vezilier, J.; Weill, M.; Read, A. F.; Gandon, S. Insecticide control of vector-borne diseases: When is insecticide resistance a problem? *PLoS Pathog.* **2010**, *6*, e1001000.

12. Ranson, H.; N'Guessan, R.; Lines, J.; Moiroux, N.; Nkuni, Z.; Corbel, V. Pyrethroid resistance in African anopheline mosquitoes: what are the implications for malaria control? *Trends Parasitol.* **2011**, *27*, 91-98.

13. World Health Organization, Global plan for insecticide resistance management in malaria vectors. World Health Organization, Geneva, 2012, (WHO/HTM/GMP/2012.5).

14. McMeniman, C. J.; Lane, R. V.; Cass, B. N.; Fong, A. W. C.; Sidhu, M.; Wang, Y. F.; O'Neill, S. L. Stable introduction of a life-shortening Wolbachia infection into the mosquito *Aedes aegypti*. *Science* **2009**, *323*, 141-144.

15. Wise de Valdez, M. R.; Suchman, E. L.; Carlson, J. O.; Black, W. C. A large scale laboratory cage trial of *Aedes* densonucleosis virus (AeDNV). *J. Med. Entomol.* **2010**, *47*, 392-399.

16. Raghavendra, K.; Barik, T. K.; Reddy, B. P. N.; Sharma, P.; Dash, A. P. Malaria vector control: From past to future. *Parasitol. Res.* **2011**, *108*, 757-779.

17. Paquette, C. C. H.; Phanse, Y.; Perry, J. L.; Sanchez-Vargas, I.; Airs, P. M.; Dunphy, B. M.; Xu, J.; Carlson, J. O.; Luft, J. C.; DeSimone, J. M.; Bartholomay, L. C.; Beaty, B. J. Biodistribution and trafficking of hydrogel nanoparticles in adult mosquitoes. *PLoS Neglected Trop. Dis.* **2015**, *9*, e0003745.

18. Fukuto, T. R. Mechanism of action of organophosphorus and carbamate insecticides. *Environ. Health Perspect.* **1990**, *87*, 245-254.

19. Colovic, M. B.; Krstic, D. Z.; Lazarevic-Pasti, T. D.; Bondzic, A. M.; Vasic, V. M. Acetylcholinesterase inhibitors: Pharmacology and toxicology. *Curr. Neuropharmacol.* **2013**, *11*, 315-335.

20. Jiang, Y.; Swale, D.; Carlier, P. R.; Hartsel, J. A.; Ma, M.; Ekström, F.; Bloomquist, J. R. Evaluation of novel carbamate insecticides for neurotoxicity to non-target species. *Pestic. Biochem. Physiol.* **2013**, *106*, 156-161.

21. Weill, M.; Lutfalla, G.; Mogensen, K.; Chandre, F.; Berthomieu, A.; Berticat, C.; Pasteur, N.; Philips, A.; Fort, P.; Raymond, M. Insecticide resistance in mosquito vectors. *Nature* **2003**, *423*, 136-137.

22. Nabeshima, T.; Mori, A.; Kozaki, T.; Iwata, Y.; Hidoh, O.; Harada, S.; Kasai, S.; Severson, D. W.; Kono, Y.; Tomita, T. An amino acid substitution attributable to insecticide-insensitivity of acetylcholinesterase in a Japanese encephalitis vector mosquito, *Culex tritaeniorhynchus*. *Biochem. Biophys. Res. Commun.* **2004**, *313*, 794-801.

23. Alout, H.; Berthomieu, A.; Hadjivassilis, A.; Weill, M. A new amino-acid substitution in acetylcholinesterase 1 confers insecticide resistance to *Culex pipiens* mosquitoes from Cyprus. *Insect Biochem. Mol. Biol.* **2007**, *37*, 41-47.

24. Gao, J. R.; Kambhampati, S.; Zhu, K. Y. Molecular cloning and characterization of a greenbug (*Schizaphis graminum*) cDNA encoding acetylcholinesterase possibly evolved from a duplicate gene lineage. *Insect Biochem. Mol. Biol.* **2002**, *32*, 765-775.

25. Weill, M.; Fort, P.; Berthomieu, A.; Dubois, M. P.; Pasteur, N.; Raymond, M. A novel acetylcholinesterase gene in mosquitoes codes for the insecticide target and is non-homologous to the *ace* gene in *Drosophila*. *Proc. R. Soc. B* **2002**, *269*, 2007-2016.

26. Huchard, E.; Martinez, M.; Alout, H.; Douzery, E. J. P.; Lutfalla, G.; Berthomieu, A.; Berticat, C.; Raymond, M.; Weill, M. Acetylcholinesterase genes within the Diptera: Takeover and loss in true flies. *Proc. R. Soc. B* **2006**, *273*, 2595-2604.

27. Kim, Y. H.; Lee, S. H. Which acetylcholinesterase functions as the main catalytic enzyme in the Class Insecta? *Insect Biochem. Mol. Biol.* **2013**, *43*, 47-53.

28. Anthony, N.; Rocheleau, T.; Mocelin, G.; Lee, H. J.; ffrench-Constant, R. Cloning, sequencing and functional expression of an acetylcholinesterase gene from the yellow fever mosquito *Aedes aegypti*. *FEBS Lett.* **1995**, *368*, 461-465.

29. Mori, A.; Lobo, N. F.; deBruyn, B.; Severson, D. W. Molecular cloning and characterization of the complete acetylcholine sterase gene (*ace1*) from the mosquito *Aedes aegypti* with implications for comparative genome analysis. *Insect Biochem. Mol. Biol.* **2007**, *37*, 667-674.

30. Carlier, P. R.; Anderson, T. D.; Wong, D. M.; Hsu, D. C.; Hartsel, J.; Ma, M.; Wong, E. A.; Choudhury, R.; Lam, P. C. H.; Totrov, M. M.; Bloomquist, J. R. Towards a species-selective acetylcholinesterase inhibitor to control the mosquito vector of malaria, *Anopheles gambiae*. *Chem.-Biol. Interact.* **2008**, *175*, 368-375.

31. Jiang, H.; Liu, S.; Zhao, P.; Pope, C. Recombinant expression and biochemical characterization of the catalytic domain of acetylcholinesterase-1 from the African malaria mosquito, *Anopheles gambiae*. *Insect Biochem. Mol. Biol.* **2009**, *39*, 646-653.

32. Zhao, P.; Wang, Y.; Jiang, H. Biochemical properties, expression profiles, and tissue localization of orthologous acetylcholinesterase-2 in the mosquito, *Anopheles gambiae*. *Insect Biochem. Mol. Biol.* **2013**, *43*, 260-271.

33. Engdahl, C.; Knutsson, S.; Fredriksson, S.-Å.; Linusson, A.; Bucht, G.; Ekström, F. Acetylcholinesterases from the disease vectors *Aedes aegypti* and *Anopheles gambiae*: Functional characterization and comparisons with vertebrate orthologues. *PLoS One* **2015**, *10*, e0138598.

34. Harel, M.; Kryger, G.; Rosenberry, T. L.; Mallender, W. D.; Lewis, T.; Fletcher, R. J.; Guss, J. M.; Silman, I.; Sussman, J. L. Three-dimensional structures of *Drosophila melanogaster* acetylcholinesterase and of its complexes with two potent inhibitors. *Protein Sci.* **2000**, *9*, 1063-1072.

35. Weill, M.; Malcolm, C.; Chandre, F.; Mogensen, K.; Berthomieu, A.; Marquine, M.; Raymond, M. The unique mutation in *ace-1* giving high insecticide resistance is easily detectable in mosquito vectors. *Insect Mol. Biol.* **2004**, *13*, 1-7.

36. Pang, Y.-P. Novel acetylcholinesterase target site for malaria mosquito control. *PLoS One* **2006**, *1*, e58.

37. Pang, Y.-P. Species marker for developing novel and safe pesticides. *Bioorg. Med. Chem. Lett.* **2007**, *17*, 197-199.

38. Pang, Y.-P.; Ekström, F.; Polsinelli, G. A.; Gao, Y.; Rana, S.; Hua, D. H.; Andersson, B.; Andersson, P. O.; Peng, L.; Singh, S. K.; Mishra, R. K.; Zhu, K. Y.; Fallon, A. M.; Ragsdale, D. W.; Brimijoin, S. Selective and irreversible inhibitors of mosquito acetylcholinesterases for controlling malaria and other mosquito-borne diseases. *PLoS One* **2009**, *4*, e6851.

39. Pang, Y.-P.; Brimijoin, S.; Ragsdale, D. W.; Zhu, K. Y.; Suranyi, R. Novel and viable acetylcholinesterase target site for developing effective and environmentally safe insecticides. *Curr. Drug Targets* **2012**, *13*, 471-482.

40. Dou, D.; Park, J. G.; Rana, S.; Madden, B. J.; Jiang, H.; Pang, Y.-P. Novel selective and irreversible mosquito acetylcholinesterase inhibitors for controlling malaria and other mosquito-borne diseases. *Sci. Rep.* **2013**, *3*, doi:10.1038/srep01068.

41. Hartsel, J. A.; Wong, D. M.; Mutunga, J. M.; Ma, M.; Anderson, T. D.; Wysinski, A.; Islam, R.; Wong, E. A.; Paulson, S. L.; Li, J.; Lam, P. C. H.; Totrov, M. M.; Bloomquist, J. R.; Carlier, P. R. Re-engineering aryl methylcarbamates to confer high selectivity for inhibition of *Anopheles gambiae* versus human acetylcholinesterase. *Bioorg. Med. Chem. Lett.* **2012**, *22*, 4593-4598.

42. Wong, D. M.; Li, J.; Chen, Q.-H.; Han, Q.; Mutunga, J. M.; Wysinski, A.; Anderson, T. D.; Ding, H.; Carpenetti, T. L.; Verma, A.; Islam, R.; Paulson, S. L.; Lam, P. C. H.; Totrov, M.; Bloomquist, J. R.; Carlier, P. R. Select small core structure carbamates exhibit high contact toxicity to "carbamate-resistant" strain malaria mosquitoes, *Anopheles gambiae* (Akron). *PLoS One* **2012**, *7*, e46712.

43. Wong, D. M.; Li, J.; Lam, P. C. H.; Hartsel, J. A.; Mutunga, J. M.; Totrov, M.; Bloomquist, J. R.; Carlier, P. R. Aryl methylcarbamates: Potency and selectivity towards wild-type and carbamate-insensitive (G119S) *Anopheles gambiae* acetylcholinesterase, and toxicity to G3 strain *An. gambiae*. *Chem.-Biol. Interact.* **2013**, *203*, 314-318.

44. Verma, A.; Wong, D. M.; Islam, R.; Tong, F.; Ghavami, M.; Mutunga, J. M.; Slebodnick, C.; Li, J.; Viayna, E.; Lam, P. C. H.; Totrov, M. M.; Bloomquist, J. R.; Carlier, P. R. 3-Oxoisoxazole-2(3H)-carboxamides and isoxazol-3-yl carbamates: Resistance-breaking acetylcholinesterase inhibitors targeting the malaria mosquito, *Anopheles gambiae*. *Bioorg. Med. Chem.* **2015**, *23*, 1321-1340.

45. Camerino, E.; Wong, D. M.; Tong, F.; Koerber, F.; Gross, A. D.; Islam, R.; Viayna, E.; Mutunga, J. M.; Li, J.; Totrov, M. M.; Bloomquist, J. R.; Carlier, P. R. Difluoromethyl ketones:

Potent inhibitors of wild type and carbamate-insensitive G119S mutant *Anopheles gambiae* acetylcholinesterase. *Bioorg. Med. Chem. Lett.* **2015**, *25*, 4405-4411.

46. Swale, D. R.; Carlier, P. R.; Hartsel, J. A.; Ma, M.; Bloomquist, J. R. Mosquitocidal carbamates with low toxicity to agricultural pests: an advantageous property for insecticide resistance management. *Pest Manage. Sci.* **2015**, *71*, 1158-1164.

47. Alout, H.; Labbe, P.; Berthomieu, A.; Djogbenou, L.; Leonetti, J.-P.; Fort, P.; Weill, M. Novel AChE inhibitors for sustainable insecticide resistance management. *PLoS One* **2012**, *7*, e47125.

48. Berg, L.; Andersson, C. D.; Artursson, E.; Hörnberg, A.; Tunemalm, A.-K.; Linusson, A.; Ekström, F. Targeting acetylcholinesterase: Identification of chemical leads by high throughput screening, structure determination and molecular modeling. *PLoS One* **2011**, *6*, e26039.

49. Ellman, G. L.; Courtney, K. D.; Andres, V.; Featherstone, R. M. A new and rapid colorimetric determination of acetylcholinesterase activity. *Biochem. Pharmacol.* **1961**, *7*, 88-95.

50. Zhang, J. H.; Chung, T. D. Y.; Oldenburg, K. R. A simple statistical parameter for use in evaluation and validation of high throughput screening assays. *J. Biomol. Screening* **1999**, *4*, 67-73.

51. Berg, L.; Mishra, B. K.; Andersson, C. D.; Ekström, F.; Linusson, A. The nature of activated non-classical hydrogen bonds: A case study on acetylcholinesterase-ligand complexes. *Chemistry* **2016**, *22*, 2672-2681.

52. Kryger, G.; Silman, I.; Sussman, J. L. Structure of acetylcholinesterase complexed with E2020 (Aricept (R)): implications for the design of new anti-Alzheimer drugs. *Structure* **1999**, *7*, 297-307.

53. Bourne, Y.; Taylor, P.; Radic, Z.; Marchot, P. Structural insights into ligand interactions at the acetylcholinesterase peripheral anionic site. *EMBO J.* **2003**, *22*, 1-12.

54. Andersson, C. D.; Forsgren, N.; Akfur, C.; Allgardsson, A.; Berg, L.; Engdahl, C.; Qian, W.; Ekström, F.; Linusson, A. Divergent structure-activity relationships of structurally similar acetylcholinesterase inhibitors. *J. Med. Chem.* **2013**, *56*, 7615-7624.

55. Berg, L.; Niemiec, M. S.; Qian, W.; Andersson, C. D.; Wittung-Stafshede, P.; Ekström, F.; Linusson, A. Similar but different: Thermodynamic and structural characterization of a pair of enantiomers binding to acetylcholinesterase. *Angew. Chem., Int. Ed.* **2012**, *51*, 12716-12720.

56. Cheung, J.; Rudolph, M. J.; Burshteyn, F.; Cassidy, M. S.; Gary, E. N.; Love, J.; Franklin, M. C.; Height, J. J. Structures of human acetylcholinesterase in complex with pharmacologically important ligands. *J. Med. Chem.* **2012**, *55*, 10282-10286.

57. Laboratories for Chemical Biology Umeå website. http://www.chemistry.umu.se/english/research/infrastructure/lcbu/ (accessed 29 June 2016).

58. Artursson, E.; Akfur, C.; Hörnberg, A.; Worek, F.; Ekström, F. Reactivation of tabun-*h*AChE investigated by structurally analogous oximes and mutagenesis. *Toxicology* **2009**, *265*, 108-114.

59. Ekström, F.; Akfur, C.; Tunemalm, A. K.; Lundberg, S. Structural changes of phenylalanine 338 and histidine 447 revealed by the crystal structures of tabun-inhibited murine acetylcholinesterase. *Biochemistry* **2006**, *45*, 74-81.

60. *GraphPad Prism*, version 6.04 for Windows; GraphPad Software: La Jola, CA, USA, www.graphpad.com, 2014.

61. *Molecular Operating Environment (MOE)*, version 2012.10; Chemical Computing Group Inc.: 1010 Sherbooke St. West, Suite #910, Montreal, QC, Canada, H3A 2R7, 2012.

62. Bylesjö, M.; Rantalainen, M.; Cloarec, O.; Nicholson, J. K.; Holmes, E.; Trygg, J. OPLS discriminant analysis: Combining the strengths of PLS-DA and SIMCA classification. *J. Chemom.* **2006**, *20*, 341-351.

63. *SIMCA-P+*, version 13.0.3; Umetrics AB: Box 7960, Umeå, Sweden, 2013.

64. *MACCS Keys*, MDL Information Systems: Inc.: 14600 Catalina Street, San Leandro, CA 94577, USA.

65. Willett, P.; Barnard, J. M.; Downs, G. M. Chemical similarity searching. *J. Chem. Inf. Comput. Sci.* **1998**, *38*, 983-996.

66. Saitou, N.; Nei, M. The neighbor-joining method - A new method for reconstructing phylogenetic trees. *Mol. Biol. Evol.* **1987**, *4*, 406-425.

67. *PHYLIP (Phylogeny Inference Package)*, version 3.6; Felsenstein, J.: Department of Genome Sciences, University of Washington, Seattle, available at: http://evolution.genetics.washington.edu/phylip.html, 2005.

68. Kabsch, W. Automatic processing of rotation diffraction data from crystals of initially unknown symmetry and cell constants. *J. Appl. Crystallogr.* **1993**, *26*, 795-800.

69. Murshudov, G. N.; Vagin, A. A.; Dodson, E. J. Refinement of macromolecular structures by the maximum-likelihood method. *Acta Crystallogr., Sect. D: Biol. Crystallogr.* **1997**, *53*, 240-255.

70. Adams, P. D.; Grosse-Kunstleve, R. W.; Hung, L. W.; Ioerger, T. R.; McCoy, A. J.; Moriarty, N. W.; Read, R. J.; Sacchettini, J. C.; Sauter, N. K.; Terwilliger, T. C. PHENIX: building new software for automated crystallographic structure determination. *Acta Crystallogr., Sect. D: Biol. Crystallogr.* **2002**, *58*, 1948-1954.

71. Emsley, P.; Cowtan, K. *Coot*: Model-building tools for molecular graphics. *Acta Crystallogr., Sect. D: Biol. Crystallogr.* **2004**, *60*, 2126-2132.

72. DeLano, W. L. The *PyMOL* Molecular Graphics System on World Wide Web http://www.pymol.org, 2002.

73. Mongin, E.; Louis, C.; Holt, R. A.; Birney, E.; Collins, F. H. The *Anopheles gambiae* genome: an update. *Trends Parasitol.* **2004**, *20*, 49-52.

74. Dvir, H.; Jiang, H. L.; Wong, D. M.; Harel, M.; Chetrit, M.; He, X. C.; Jin, G. Y.; Yu, G. L.; Tang, X. C.; Silman, I.; Bai, D. L.; Sussman, J. L. X-ray structures of *Torpedo californica* acetylcholinesterase complexed with (+)-Huperzine A and (-)-huperzine B: Structural evidence for an active site rearrangement. *Biochemistry* **2002**, *41*, 10810-10818.

75. Larkin, M. A.; Blackshields, G.; Brown, N. P.; Chenna, R.; McGettigan, P. A.; McWilliam, H.; Valentin, F.; Wallace, I. M.; Wilm, A.; Lopez, R.; Thompson, J. D.; Gibson, T. J.; Higgins, D. G. Clustal W and Clustal X version 2.0. *Bioinformatics* **2007**, *23*, 2947-2948.

76. *Molecular Operating Environment (MOE)*, version 2014.10; Chemical Computing Group Inc.: 1010 Sherbooke St. West, Suite #910, Montreal, QC, Canada, H3A 2R7, 2014.

77. Labute, P. Protonate3D: Assignment of ionization states and hydrogen coordinates to macromolecular structures. *Proteins: Struct., Funct., Bioinf.* **2009**, *75*, 187-205.

78. Summa, C. M.; Levitt, M. Near-native structure refinement using in vacuo energy minimization. *Proc. Natl. Acad. Sci. U. S. A.* **2007**, *104*, 3177-3182.

79. Wang, J. M.; Cieplak, P.; Kollman, P. A. How well does a restrained electrostatic potential (RESP) model perform in calculating conformational energies of organic and biological molecules? *J. Comput. Chem.* **2000**, *21*, 1049-1074.

80. Berman, H. M.; Westbrook, J.; Feng, Z.; Gilliland, G.; Bhat, T. N.; Weissig, H.; Shindyalov, I. N.; Bourne, P. E. The protein data bank. *Nucleic Acids Res.* **2000**, *28*, 235-242.

81. Labute, P. The generalized Born/volume integral implicit solvent model: Estimation of the free energy of hydration using London dispersion instead of atomic surface area. *J. Comput. Chem.* **2008**, *29*, 1693-1698.

82. *Maestro*, version 10.3; Schrödinger, LLC: New York, NY, USA, 2015.

83. Polak, E.; Ribiere, G. Note on the convergence of methods of conjugate directions. *Revue Francaise d'Informatique et de Recherche Operationnelle* **1969**, *3*, 35-43.

84. Kaminski, G. A.; Friesner, R. A.; Tirado-Rives, J.; Jorgensen, W. L. Evaluation and reparametrization of the OPLS-AA force field for proteins via comparison with accurate quantum chemical calculations on peptides. *J. Phys. Chem. B* **2001**, *105*, 6474-6487.

85. *Macromodel*, version 10.1; Schrödinger, LLC: New York, NY, USA, 2013.

86. Laskowski, R. A.; Macarthur, M. W.; Moss, D. S.; Thornton, J. M. PROCHECK: A program to check the stereochemical quality of protein structures. *J. Appl. Crystallogr.* **1993**, *26*, 283-291.

87. Halgren, T. A. MMFF VII. Characterization of MMFF94, MMFF94s, and other widely available force fields for conformational energies and for intermolecular-interaction energies and geometries. *J. Comput. Chem.* **1999**, *20*, 730-748.

88. Labute, P.; Williams, C.; Feher, M.; Sourial, E.; Schmidt, J. M. Flexible alignment of small molecules. *J. Med. Chem.* **2001**, *44*, 1483-1490.

89. *Macromodel*, version 10.9; Schrödinger, LLC: New York, NY, USA, 2015.

## Table of Contents Graphic

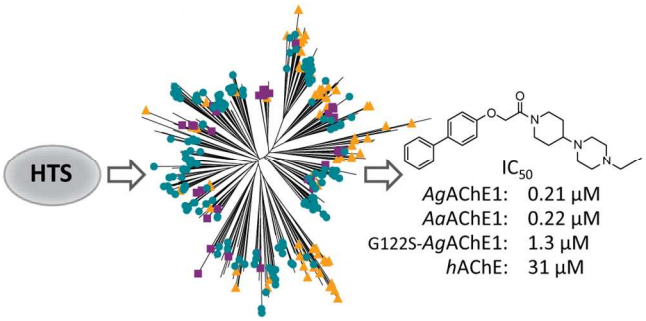

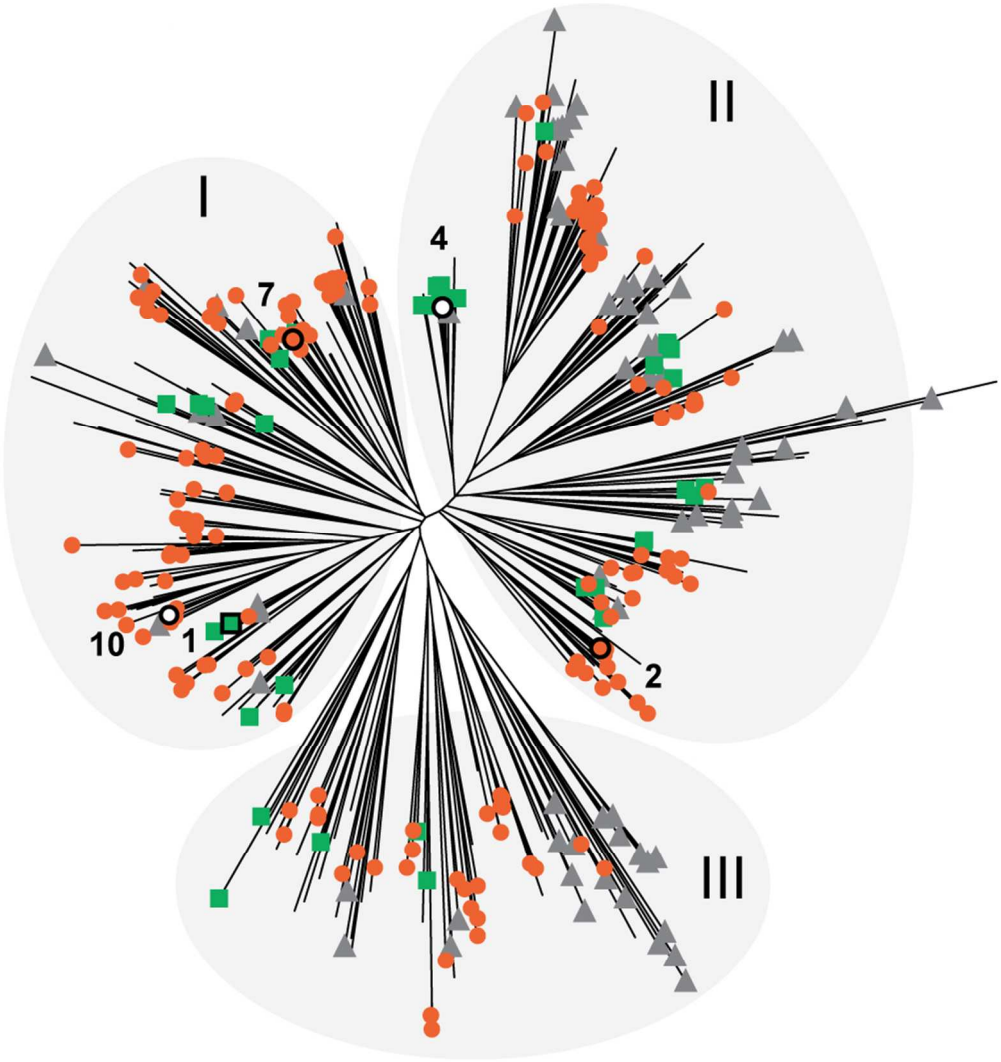


Figure 2. Chemical structural tree of the 425 AChE1 and hAChE hits. Three major classes (I-III) of hits are shown, each against a grey background. Based on the HTS-data, hits showing potential selectivity for AChE1 are shown as orange dots, non-selective hits as green squares, and hits showing potential selectivity for hAChE as grey triangles, while non-marked hits were miscellaneous. Compounds 1, 2, 4, 7, and 10 are labeled and their symbols are outlined in black.

84x90mm (300 x 300 DPI)

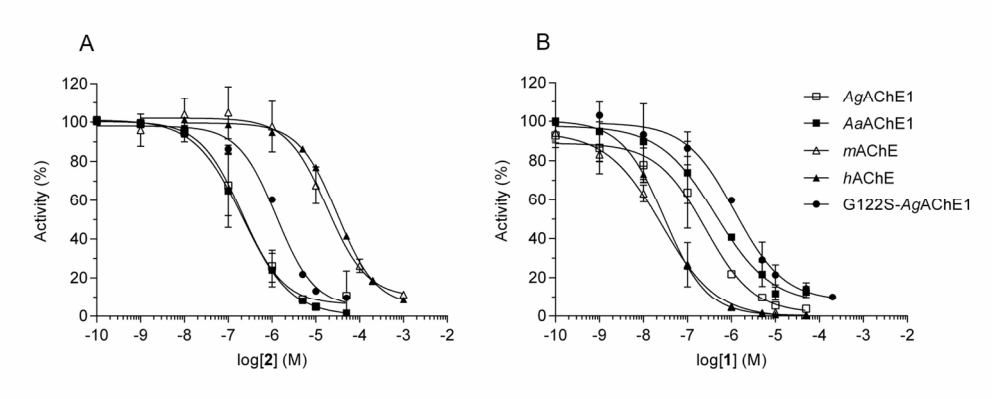


Figure 3. Dose-response curves for compounds 2 (A) and 1 (B). The plotted results are means ± standard deviations based on 2-3 measurements. IC50-values against Ag-, AaAChE1, and hAChE are presented in Table 2; for compounds 2 and 1 the IC50-values for mAChE were 18 (8.7-38) μM and 0.026 (0.018-0.039), respectively, and for G122S-AgAChE1 1.3 (0.98-1.7) μM and 1.2 (0.77-1.9) μM, respectively.

68x27mm (600 x 600 DPI)

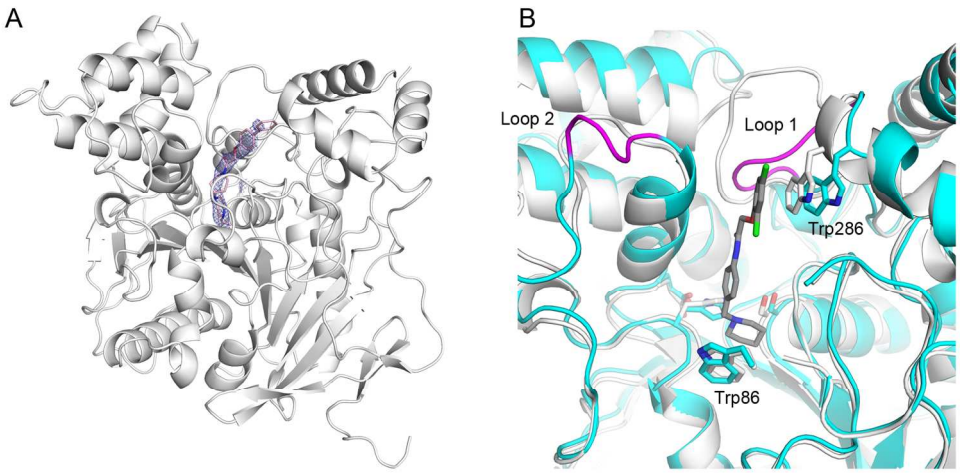


Figure 4. Structures of enzyme-inhibitor complexes. (A) Crystal structure of 2•mAChE (pdb code: 5FUM) with compound 2 in pink and its electron density shown in blue (simulated annealing Fo-Fc omit map at 3 σ). (B) Homology model of AgAChE1 shown in cyan superimposed to 1•mAChE (pdb code: 5FOQ) in white. The two loops at the entrance of the gorge responsible for the main differences between AgAChE1 and mAChE are highlighted in magenta.

160x78mm (300 x 300 DPI)

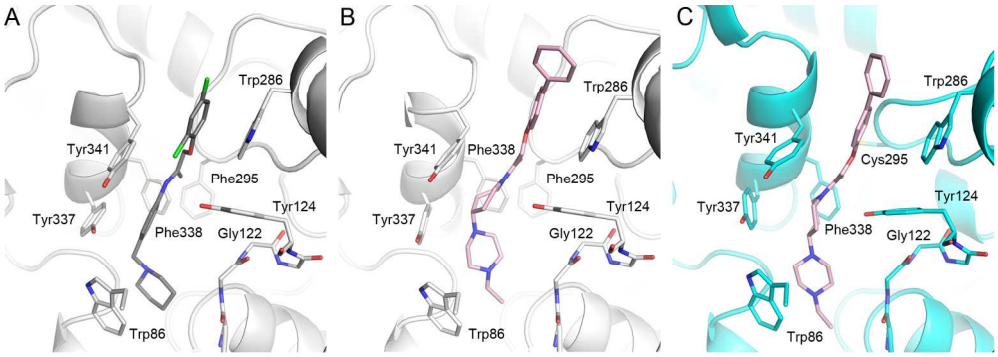


Figure 5. Binding poses of inhibitors in the active site gorge of mAChE (A-B; pdb codes: 5FOQ and 5FUM) and AgAChE1 (C, homology model). The structures of mAChE and AgAChE1 are shown in white and cyan, respectively; compounds 1 and 2 are shown in grey and pink, respectively.

177x61mm (300 x 300 DPI)

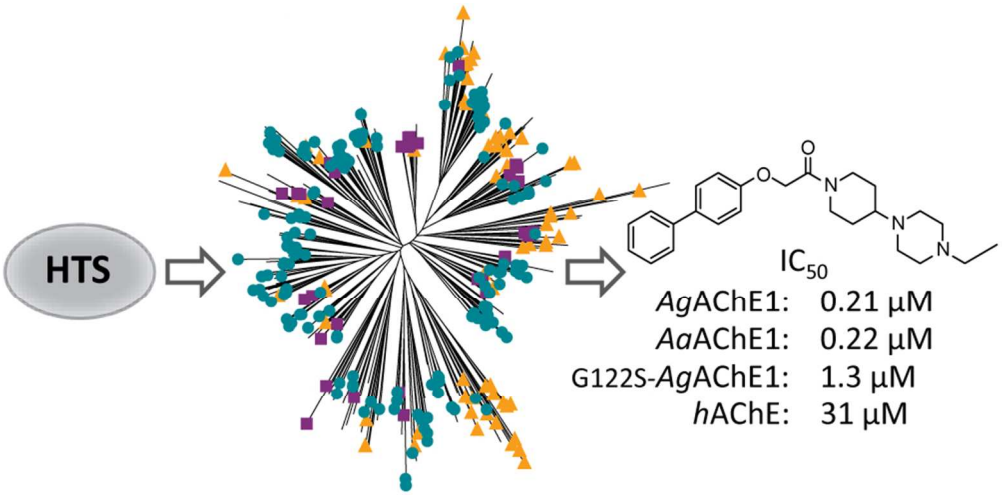


Table of Contents Graphic

85x41mm (300 x 300 DPI)